UNIVERSITÀ DEGLI STUDI DI NAPOLI
FEDERICO II

UNIVERSITY OF NAPLES " FEDERICO II''

PH.D. THESIS IN

INFORMATION TECHNOLOGY AND ELECTRICAL ENGINEERING

Control Strategies and Design to Range in Light Railway Systems

PH.D. THESIS OF **DOMENICO PERNA**

COURSE XXIX

TUTOR:
Prof. Andrea Del Pizzo

PH.D. COORDINATOR:
Prof. Daniele Riccio

CO-TUTOR:
Ph.D. Eng. Luigi Fratelli

POLYTECHNIC **S**CHOOL AND **B**ASIC **S**CIENCES

DEPARTMENT OF **E**LECTRICAL **E**NGINEERING AND **I**NFORMATION **T**ECHNOLOGY

MARCH 2017

Index

List of symbols and acronyms

a: 1st coefficient of the motion resistance

b: 2nd coefficient of themotion resistance

F_{Tr} : Effort of the vehicle

f_{sw} : Switching frequency

I : Current amplitude

i_{dc-dc} : dc/dc converter current

i_{Dr} : dc current of the propulsion unit

i_{Lin} : Substation current

i_{SC} : Supercapacitors stack current

i_{sd} : d-axis component of the state current space vector

i_{sq} : q-axis component of the state current space vector

$k_{P,c}$: Proportional constant of PI compensation regulator

$k_{I,c}$: Integral constant of PI compensation regulator

$k_{P,i}$: Proportional constant of PI Supercapacitors current regulator

$k_{I,i}$: Integral constant of PI Supercapacitors current regulator

$k_{P,V}$: Proportional constant of PI dc/dc Converter voltage regulator

$k_{I,V}$: Integral constant of PI dc/dc Converter voltage regulator

$k_{P,\omega}$: Proportional constant of PI adaptive law

$k_{I,\omega}$: Integral constant of PI adaptive law

l_{tot} : total length of the path simulated with variable resistor

L_d : d-axis self inductance

L_q : q-axis self inductance

L_m : Motor air-gap inductance

$L_r^{'}$: Rotor phase inductance referred to the stator

L_s : Stator phase inductance referred to the stator

$L_{\sigma r}^{'}$: Rotor phase leakage inductance referred to the stator

$L_{\sigma s}$: Stator phase leakage inductance

P : Pole pairs number

P_{Ch} : Braking Chopper power

P_{Dr} : Propulsion Unit power

P_{Lin} : Substation power

P_m : Mechanical power

P_{SC} : Supercapacitors Stack power

R_s : Stator phase resistance

R'_r : Rotor resistance referred to the stator

R_{SC} : Internal equivalent resistance of the Supercapacitors Stack

$R_1(x)$: Equivalent resistance from the Electrical Substation to the Vehicle

$R_2(x)$: Equivalent resistance from Supercapacitors to the Vehicle

R_{tot} : Equivalent total resistance

T_e : Electromagnetic torque

V : Voltage amplitude

v_{Dr} : DC voltage of the propulsion unit

v_{Fil} : Voltage of dc/dc converter

v_{Lin} : Substation voltage

v_{SC} : Supercapacitors stack voltage

v_{sd} : d-axis component of state voltage space-vector

v_{sq} : q-axis component of state voltage space-vector

v_{Tr} : Speed of the vehicle

W_{Ch} : Braking Chopper energy

W_{Dr} : Propulsion Unit energy

W_{Lin} : Substation energy

W_{SC} : Supecapacitors Stack energy

$W_{Vehicle}$: Vehicle energy

δ : duty cycle

ϕ_{sd} : d-axis component of state rotor flux space-vector

ϕ_{sq} : q-axis component of state rotor flux space-vector

η_{Dr} : Propulsion Unit efficiency

η_{Gear} : Mechanical gear box efficiency

η_{SC} : Supercapacitors stack efficiency

ω_r : Mechanical rotor angular speed

$\omega_{r,e}$: Electrical rotor angular speed

ω_σ : Slip angular speed

ω : Instantaneous angular speed

superscript*: reference

superscript^: estimated

subscript C: charge

subscript D: discharge

subscript L: limit value

ES : Electrical SubStation

ESS : Energy Storage System

EDLC: Electric Double-Layer Capacitor

LRT : Light Railway Transportation

SC : Supercapacitor

SESS : Supercapacitors Energy Storage System

List of figures

Fig. 3.26) Time behaviour of Torque and rotor speed error of PM unit with the decrease of 10% for L_s and R_s

Fig. 3.27) Time behaviour of Torque and rotor speed error of PM unit with the decrease of 20% for L_s and R_s

Fig. 3.28) Time behaviour of Torque and rotor speed error of IM unit with the increase of 10% for R_s, $R_r^{'}$ and L_m

Fig. 3.29) Time behaviour of Torque and rotor speed error of IM unit with the increase of 20% for R_s, $R_r^{'}$ and L_m

Fig. 3.30) Time behaviour of Torque and rotor speed error of IM unit with the decrease of 10% for R_s, $R_r^{'}$ and L_m

Fig. 3.31) Time behaviour of Torque and rotor speed error of IM unit with the decrease of 20% for R_s, $R_r^{'}$ and L_m

List of tables

Introduction

In general, a *Transportation System* can be defined as the combination of elements and their interactions, which produce the demand for travel within a given area and the supply of transportation services to satisfy this demand [1].

In Europe, *Transport* is accountable for about 25% of greenhouse gas emissions, with 12.7% of the global emissions due to civil aviation, 13.5% by maritime transport, 1.7% by inland navigation, and 71.4% by road and rail transport [2].

Transport White Paper of the European Commission 2013 has been adopted as a objective for the reduction of greenhouse gas emissions from transport at least of 60% by 2050, compared to 1990 levels. Due to the fact that the emission of rail transport is at least 3-4 times lower than road or air-transport, it is easy to forecast the important role that rail transport can play in reaching the 2050 target [2].

Public Transport (also called transit, public transit, or mass transit) is defined as the transportation by a conveyance that provides regular and continuing general or special transportation of the people, but not including school buses, charter or sightseeing services [3].

In Europe, Public Transport in urban areas represents 21% of motorized mobility and is responsible for roughly 10% of transport-related greenhouse gas emissions [2].

Rail is also a fundamental part of the Public Transport which consumes 3.7 times less energy per passenger transported in Europe than private car; compared to air travel and automobiles in Europe, trains are the most friendly passenger transport mode

in terms of energy consumption, CO2 and exhaust atmospheric emission and then the need of transport in the rail context is even more evident [2]. Thus, the spread in all major cities of railway *urban transport systems* (see Figure1.1), consisting of a combination of suburban and regional conventional rail lines, metro, tram and light rail networks, allowed to help the cities to better manage their transport energy consumption and pollution.

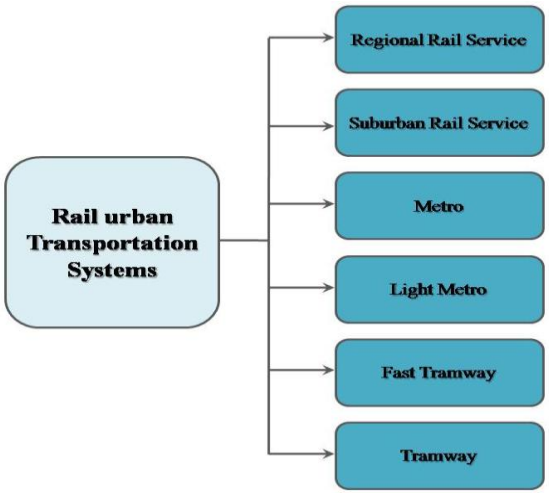

Figure 1.1 **Description of urban transportation systems**

Important parameters for the classification of these various systems are the rate of passengers per hour, average and maximum speeds, distances covered and overall travel speed. In Figure 1.2 is drawn a *Light Railway System* considered in the next developments.

Figure 1.2 **View of Light Railway System**

Nevertheless, the railway transportation is a multidisciplinary area of interest with many different and complex perspectives. Since their spread is continuously growing, the future of rail transport will be characterized by competition with other carriers in terms of costs, energy efficiency and environmental compatibility. Therefore the introduction of new solutions able to improve efficiency, costs, reliability and security of the various subsystems of the railway vehicles is mandatory in order to meet the continuously evolving market challenges. In Figure 1.3 are highlighted different ways for improvements concerning energy efficiency and reliability in rail transport.

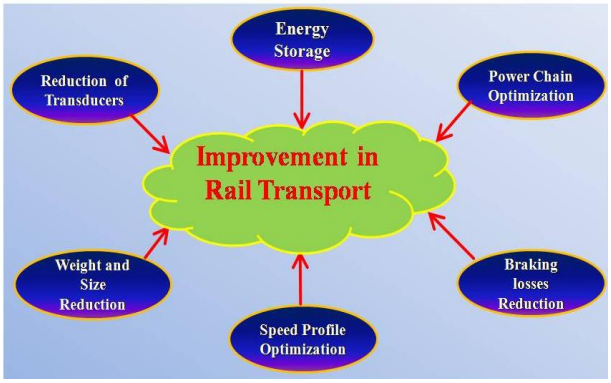

Figure 1.3 **Possible improvements in rail transport**

The traction units are obviously the core of railway vehicles as responsible of the electromechanical energy conversion. During the years, the architecture of the propulsion units has been closely linked to the evolution of the different technologies belonging to the railway traction context. The development of power electronics has made convenient the use of induction motor (IM) drives which are still the most used in railway propulsion, mainly thanks to the unquestionable advantages of the motors in terms of construction simplicity, intrinsic reliability and robustness, relatively low cost ([5] , [15]).

However, permanent magnet (PM) synchronous motor (SM) drives are more and more considered for railway traction applications ([4], [6]), especially because of their high power density and efficiency; further advantages are high values of power factor and low values of rotor temperature, combined with acceptable reliability levels.

In the last decade, permanent magnet brushless drives are gaining market share in traction drives due to expected higher efficiency e lower sizes and weight, but some typical problems are slowing down their widespread.

In the technical literature several analyses are performed between IM and PMSM drives for rail traction units. They are mainly focused on sizes and weight, efficiency, dynamic response, reliability, limitation in the operating dominion, overloading capability, possibility to remove gear (or reduce gear ratio), power quality indexes on the feeding line, possibility to provide one inverter for two o more motors, cooling system, protections, behavior in case of failure [6]÷[17].

From the point of view of the traction control, most of the manufacturers of railway traction units are now using vector control of IM or PMSM drives, even if different choices are made (e.g. FOC--Field Oriented Control or SV-DTC--Space Vector modulated Direct Torque Control, ..). It ensures good dynamic and energetic performance, satisfactory stability and high values of power quality indexes both in the drive and in the feeding catenary, as required by modern propulsion systems [14].

The optimization of the speed profile of the vehicle is another important topic and have been object of different studies [18]÷[21]. Changing drive train operations, is possible to increase energy saving for the whole railway system, which results in the same trip distance with equivalent stops and in the same final time, but with lower energy consumption (Eco-Driving). There were many studies on optimal speed profile and in particular some paper [19] dealt with optimization of speed-time diagram by controlling the duration of inertial slowing down phase, also called "coasting".

Nowadays, one of the most effective way to improve the energy efficiency is the recovery of energy during the braking phase of the vehicle. In case of non receptive DC grid, is possible to recover the total amount of the energy regenerated only if there is another vehicle in acceleration phase. Otherwise the energy is wasted on the braking resistor [24]. For this reasons, energy storage system is the main tool to improve energy efficiency in railway systems and design methods and control schemes for ESS are constantly being improved, which is bringing new possibilities to the railway sector [23] ÷ [26].

Among different complexities of railway system with particular attention to the traction units, the researchers have been focused also on finding solutions for the elimination of transducers (i.e., one of the three adopted for stator currents or the one used for current of the braking chopper). Besides, also the presence of conventional and accurate speed sensors or position sensors (i.e. PM brushless drives) is more and more considered undesired not only due to their cost but mainly because they may involve problems in terms of reliability, due to their critical positioning ([27],[28]). Therefore, their elimination may involve in benefit as downsizing and lightweight of the traction motor, increasing reliability of the traction system and reducing costs.

In this thesis will be presented control strategies and a design method to carry out at different levels improvements in railway field in terms of energy efficiency and reliability. More in detail, the investigations will be focused on the possibility to use ESSs in light railway systems. Thanks to a preliminary analysis of the storage technologies available on the market, Supercapacitors ESS will be considered *on board* of a real vehicle, with the purpose of introduce a methodology for design to range of SESS in order to achieve different routes in conditions of power supply gaps. Also *stationary* configuration of SESS will be considered, with the aim of introduce a control strategy for energy flows management in non receptive DC grid. Furthermore, will be evaluated the possibility of introduce two sensorless control strategies for two different railway traction architectures with IM and PMSM drives, taking into account energetic aspects and specific dynamic performance required to the railway traction drives.

The following chapters are divides as:

Chapter 1: Introduction and comparison of different technologies for ESSs in Railway Transportation field.

Chapter 2: Introduction of a method for Design of SESS on board of a prototype light rail vehicle in conditions of power supply gaps and the introduction of a Control Strategy of SESS in Stationary configuration for energy flows management in light railway systems.

Chapter 3: Introduction of two Sensorless control strategies for a real railway vehicle taking into account two different railway traction architecture with IM and PM brushless drives.

Chapter 1

Review on hybrid light railway transportation systems

Light Rail is a particular tram system, utilized for urban and suburban passengers transport that allows higher speed values and higher flow rates compared to *Tram.*

Energy saving and *clean energy sources* receive even more interest especially in urban transportation field, due to the concerns for environmental conservation and uncertain future state of energy resources. As aforementioned, while these mass transit systems enable large reductions in terms of emissions, their energy efficiency could be significantly improved. In other words, to enhance the environmental advantages and improve power regeneration and energy supply throughout the railway system, further optimizations on energy consumption are needed.

In particular, one key to carry out these improvements for the railways can be represented by the *hybridization* of their power system with the inclusion of the ESSs [29]÷ [32].The introduction of ESSs, *on-board* of the vehicle or *stationary* in a specified point of the track or at the level of the substation, may increase the global efficiency of the system, for example by storing the braking energy otherwise lost or operating in support of the power line. Another possibility for the vehicle could be represented by the overcoming of gaps in power supply.

In the next paragraphs different ESSs technologies for railway applications are discussed and more detail will be provided about *Supercapacitor* storage system.

1.1 Different technologies for ESSs in Railway applications

As before mentioned, urban transportation is an effective way to substantially reduce the overall emissions and improving energy efficiency .

In general, the advantage of using ESSs in electrified railways is mainly represented by the reuse of the energy coming from vehicle while braking. If the power supply is receptive, the braking energy is fed back to the AC grid; otherwise, in case of standard DC railways without this possibility, the energy could be provided to another vehicle only if this vehicle is present and is accelerating. However, this situation is infrequent and often most of the remaining braking energy is dissipated by a braking rheostat or by mechanical braking. In Barrero et al. works, have been addressed the evaluations of the benefits derived by the introduction on-board of ESSs in a light tram system with good results [33], and a similar analysis has been conducted for stationary ESSs in a metro system [34].

Electrified vehicles with an *on-board energy storage* elements have the possibility to store the electrical energy from the grid or derived by kinetic energy, reusing it in order to perform *energy saving*, *power supply optimization* or *catenary-free operations*.

Instead, *stationary ESSs* contribute also to the improvement of *energy efficiency* associated with the reduction of the power delivery rate by *power peak shaving* and a global improvement in the *power quality* for the whole transportation system.

For these reasons, the choice of the ESS is linked in case of *on-board equipment* to the requirements of the railway vehicle,

such as: 1) efficiency; 2) load capability; 3) weight and size. In fact, for vehicles who performs long distances with few stops, this solution could be more preferable.

Otherwise, in *wayside applications*, is directly correlated to the characteristics of DC - electrified system and the position of ESSs, i.e. , either if the substation is or not regenerative or ESSs are placed in the substation rather than in a specific section along the path. This application could be more interesting in urban transport, because of the high frequency of the service.

At follow a generic classification is carried out on the basis of the main technologies mostly used in railway field, that is:

- Batteries
- Flywheels
- Supercapacitors

and characteristic data of some of these ones are summarized in Table 1.1 [35] ÷ [44].

Regarding the *Batteries*, these are the oldest and still the most widely used system for energy storage. They have been used in electrified railways in Japan were lead-acid type were arranged in battery posts, installed in parallel with the power substation, with the aim of a reduction of energy demand and a support of the power supply system for a short time in case of a fault [38]. The different types, such as Lead acid, Nickel Cadmium (NiCd) or Nickel Metal (NiMH) have high energy density but low power density; consequently, they are not suitable to be charged/ discharged in a very short time. In addition, their limited life is further reduced if deep charge/discharge operations occur. This

makes difficult to use batteries for energy recovery in urban/suburban railway vehicles, where starting/braking operations are frequently requested in short time intervals.

TABLE 1.1 **Features of energy storage systems**

Parameters	**Li-Ion Battery**	**Zebra Battery**	**Double -Layer Supercapacitor**	**Li – Ion Supercapacitor**	**Flywheel**
Energy Density[*Wh/kg*]	100 ÷ 200	50 ÷ 150	5 ÷ 8	10 ÷35	5 ÷ 50
Power Density[*kW/kg*]	0.1÷1	0.1÷0.2	2 ÷ 5	1÷2	0.18 ÷ 1.8
Life time [years]	4 ÷ 6	2.5÷ 5	10 ÷ 15	10 ÷ 15	~20
Number of cycles	500 ÷ 2000	1000 ÷ 2000	$0.1\ 10^6 \div 10^6$	$0.1\ 10^6 \div 10^6$	$3\ 10^6$
Efficiency[%]	70 ÷ 85	70 ÷ 90	85 ÷ 98	85 ÷ 98	90 ÷ 95
Time of charge/discharge	Minutes to hours	Minutes to hours	0.3÷30 seconds	0.3÷30 seconds	Seconds to minutes
Technological Maturity	High	High	Medium	Medium	Medium

Lithium-ion batteries have been used several times for enhancing energy efficiency in Japanese electrified railways with same very interesting result [38],[39],[40]. In Lithium-Ion technology, the main advantages are high energy-to-weight ratios, no memory effect and a low self-discharge. However, the price of these batteries is still high and despite the cell of this battery can be operated with high current levels, the internal resistance can produce internal heat-up and failures; due to the presence of Lithium element , there is also an high risk of fire.

ZEBRA is a kind of high-energy battery made from common salt, ceramics, and nickel. Important gains of this technology are high current levels and no self-discharge phenomena. Another important feature is since they operate at ~300°C, there are no detrimental effects resulting from their use at extremely cold or hot ambient temperature. Besides, the high operating temperature forces a fraction of energy to be used to maintain this operating

temperature, resulting in a lower overall efficiency. Examples of vehicles with Zebra batteries on board are pure electric and hybrid electric battery buses in service in the Italian cities of Bologna, Firenze, and Modena [41].

Also *Flywheels* have been object of different studies in the last decades [38],[42],[43], were at first they have been installed in Japan in the Keihin Electric Express Railway for energy saving purpose [39]. With respect to the batteries, modern high speed *flywheels* have lower energy density but higher power density, life length and efficiency (see Table 1.1). Charge/discharge times are really short and fast enough to meet the requirements of braking power recovery (some seconds) in urban railway applications. Nevertheless the high maintenance required and the safety in case of accident are the most relevant disadvantages in transportation systems.

Every one of the major company operating in railway field has conducted research and development, carrying out tests on the real vehicle to verify the performance of their product with the use of EDLC [38]. Very high power density and very large number of allowed charge/discharge cycles are the main features of current *double-layer supercapacitor*s (see Table I). Consequently, they are suitable to be used either as on-board or stationary ESS especially to efficiently recovery braking power and to support feeding line of railway vehicles. On the contrary, energy density in supercapacitors is considerably lower than in the batteries, therefore their use as energy source for catenary-free operations implies the use of an ESS with a quite large volume and weight.

Also the *lithium-ion super-capacitors* (LiC) have to be taken under consideration for the use in hybrid railway vehicles, due to their promising properties. Developed in the last years, they are characterized by an efficiency and charge/discharge features similar to the standard supercapacitors, but with lower leakage current and with values of energy density and power density intermediate between batteries and standard super-capacitors. Using only small amount of lithium, these devices do not have the fire hazard of lithium batteries. However, thermal resistance problems occurs when they operate at high temperature.

After these considerations, the choice of ESS able to meet the challenges previously discussed has been directed toward *double-layer supercapacitors* and the next paragraph give a brief overview about their physical structure, electrical modeling adopted and construction details.

1.2 Supercapacitors ESS

As well known, *conventional capacitors* are made of two conducting electrodes separated by a dielectric material. Applying a voltage to a capacitor, opposite charges accumulate on the surfaces of each electrode. The charges are electrically separated by the dielectric and then producing an electric field that allows to the capacitor to store energy.

The capacitance C of a conventional capacitor, is proportional directly to the surface area S of each electrode and inversely to the distance d between the electrodes through the well-known equation:

$$C = \varepsilon_0 \varepsilon_r \cdot \frac{S}{d} \qquad (1.1)$$

The dielectric is considered through the product of ε_0 which is the dielectric constant (or "permittivity") of the vacuum and ε_r ,who represent the dielectric constant of the insulating material between the electrodes. Conventional capacitors have a relatively high power densities, but relatively low energy densities if they are compared to batteries and fuel cells.

Supercapacitors, also known as ultracapacitors, are ruled by the same basic principle but to fulfill capacitances several orders of magnitude larger than conventional capacitors they utilize greater surface area for the electrodes and thinner electrolytic dielectrics.

H. Helmholtz was the first who observed the phenomenon which describes the performance of Supercapacitor ([45],[46],[46],[47],[48]). In Figure 1.4 is pointed out a single cell of electric double layer capacitor (EDLC).

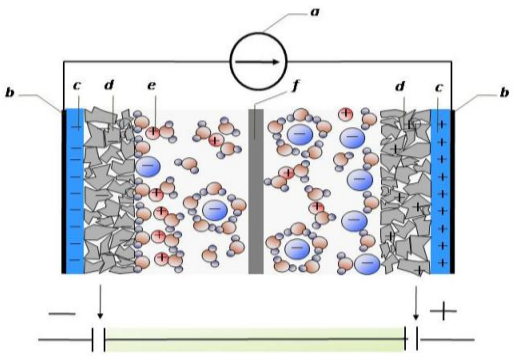

Figure 1.4 **EDLC cell : a) Charger; b) Current Collectors; c) Polarized electrodes; d) Helmholtz Electric Double Layer; e) Electrolyte solutions; f) Separator**

The Helmholtz studies has led to double layer differential capacitance as expressed in (1.1), while Gouy and Chapman have defined the double layer differential capacitance as:

$$C_{g-c} = z\sqrt{\frac{2qn_0\varepsilon}{u_t}}\cosh\frac{z\Psi_0}{2u_t} \qquad (1.2)$$

This result has been achieved through the mathematical formulation of the charge by means of a Poisson equation and Boltzmann distribution, where ε is the absolute dielectric constant, z is the valence of the ions, n_o is the number of ions per cubic meter, Ψ_o is the applied potential drop, q is the elementary charge and u_t is the thermodynamic potential, so defined:

$$u_t = \frac{kT}{q} \qquad (1.3)$$

where T is the temperature (in Kelvin degree) and k the Boltzmann constant. Instead, Stern used a mixed approach dividing the double layer in two zones: a first area according to Helmholtz theory considering that the potential distribution is linear and the second one where the charge distribution is a double diffusion layer, leading at least in the solution:

$$\frac{1}{C_s} = \frac{1}{C_h} + \frac{1}{C_{g-c}} \qquad (1.4)$$

Several evolutions have been developed starting from all these electrochemical models, taking into account different typologies of the electrodes and electrolytes; also different design technique aimed to maximize surface area of the double layer has been proposed ([49],[50]). Hence these investigations have involved in more electrical models [51]÷ [53] and in Figure 1.5 is drawn

the electrical model adopted in the studies carried out in this thesis.

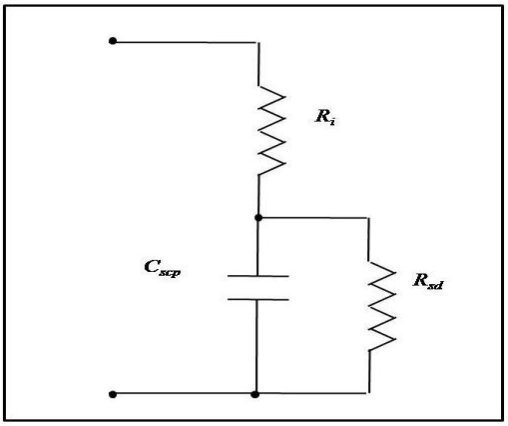

Figure 1.5 **Series/Parallel Model**

In this model, a lumped ideal equivalent capacitance (C_{scp}) is connected with an equivalent series resistance (R_i) which synthesizes internal model resistance and an equivalent parallel resistance (R_{sd}) to consider the current leakage taking into account self-discharge phenomena[55].The simplicity of this model makes his use suitable for model and control exploitations during the steady state operations , but during the SC transients of charge/discharge, the above model fails because the non-linear behavior of the SC is not taken into account.

For transport and industry, SC are assembled in modules consisting of elementary cells connected in series and parallel to increase both voltage and the overall capacitance. To avoid the unbalancing within the voltages of the cells, they are usually provided by active electronic systems. In Figure 1.6, a Maxwell module for traction applications is depicted with rated values of capacitance of 63F and 125V DC voltage [54].

Figure 1.6 **Maxwell BMOD0063 P125 SC module**

It is worth of remark that their suitability in transport is mainly due to the fact that they offers the chance of recovery and release energy in an high reversible way while the efficiency is not affected by the number of charge/discharge cycles; however, current limitation is needed because of low value of internal resistance.

An important issue for the use of storage systems is the monitoring of state of charge (SoC): respect to the case of batteries , for a SC the evaluation of SoC is quite easy because if it is assumed that the capacitance is kept constant, the energy is directly linked to the measurement of voltage at terminals.

In fact the energy stored is proportional to the value of equivalent capacitance and the square of voltage and either, in charging or discharging phases, the voltage at terminals is directly related to the SoC. This leads that SCs are not able to provide all the charge stored, because below a certain value of SoC the terminal voltage decrease at values which not permit the correct performance of ESS.

Chapter 2

Design and Energy management of Supercapacitors in Light Railway Systems

It should be clear that the introduction of SESSs would increase the global efficiency of the systems, by considering the possibilities of use these equipments *on-board* of the vehicle or *stationary* (i.e., in substation or wayside applications) , as it is widely shown in the technical literature ([33],[34],[38],[42]).

Several benefits can be achieved for the railway system in both cases and these improvements can be synthesized as follow:

- *energy saving* (storing kinetic energy while braking and reusing it to support acceleration phases of vehicle);
- *losses reduction* on feeding line;
- *voltage profile optimization*;
- *peak shaving* (using stored energy to reduce peak current in catenary system);
- *catenary-free operation* (using previously stored energy to fill gaps in power supply).

However, the use of stationary configuration with respect to an on-board solution, may involves in the decreasing of losses reduction along supply line ; or in lower amount of energy recovered because of some braking chopper operation and still in the lack of opportunity for a single vehicle to operate in catenary-free mode.

Otherwise, the disadvantages of on-board solutions compared to stationary applications, are mainly due to the size, weight and volume of SESSs employed on-board of the vehicle; furthermore, maintenance operations may affect service frequency of the transport and in case of fire they represent a risk for passengers.

Nevertheless in the next sections will be discussed the efforts of our investigations arranged as follow, that is:

1) find an optimal strategy to design the whole capacitance needed for SESSs on board of vehicle, in order to realize distinct routes with different speed-time diagrams and slopes in catenary-free operations;

2) introduce a control strategy in stationary configuration of SESS to realize the improvements above discussed in terms of *energy saving*, *power peak shaving* and *voltage profile optimization* for the railway system.

2.1 Design to range of SESSs in Catenary-free operations

Sometimes the vehicles can operate along some distances in catenary-free mode in order to satisfy two main requirements:

- safety, for moving vehicles to a station in case of catenary line fault;
- conservation of old towns, avoiding the presence of catenary in historical places and important cultural heritages ([55],[38]).

Usually, catenary-free operation is carried out at quite low speed because the goal is not intended in terms of performance

but in terms of crossing the gap without power supply. Hence, all the subsystems of the vehicle work in operating conditions different from the rated ones and consequently the vehicle efficiency, losses and dynamic parameters assume different behaviors in this situation. Indeed, as it is known, motor and inverter losses at start-up are much larger than rated ones due to the higher current values and high switching frequency; on the other side, at low speed, the losses due to the mechanical gear, friction and ventilation are lower than the rated ones.

Besides, the large weight and volume needed on board of vehicle for SESSs determines the deterioration of dynamic performance and the increase of the space necessary for the installations of the system, therefore the oversizing of SESSs must be avoided and the storage capacity must be limited to the minimum value required by the catenary-free path mission which has to be properly estimated: at this purpose the development of an accurate energetic model of the vehicle is crucial.

Thus in order to obtain an optimized sizing procedure, it is possible to use an energetic model of the system pointed out by means of several experimental measurements carried out on a real vehicle which operates in different line-disconnected operating conditions.

2.1.1 Configurations of on board Power Conversion System with SESS

The energetic analysis that will be conducted in the following refers to the schematic electrical diagram in Figure 2.1. It represents a part of the on-board power conversion unit of a real tram for both traction and auxiliary apparatuses; however, this architecture can be used for any railway vehicle.

We can recognize a 3-ph PWM-VSI devoted to on-board auxiliary services, two 3-ph PWM-VSIs feeding two induction motors in parallel for traction, a dc-dc converter as interface of supercapacitor stacks versus the dc-link. For all considered VSIs the power devices are IGBTs. Really, the whole power conversion circuit of the vehicle includes another VSI for on-board auxiliary services and other two motors supplied by two traction converters in parallel on the same dc-link DB of Fig.2.1. Only the blocks "supercapacitor stacks" and "dc/dc converter" of Fig.2.1 are not duplicated in the whole power circuit. In ordinary catenary-connected operations, these supercaps store and return energy during braking or starting phases respectively.

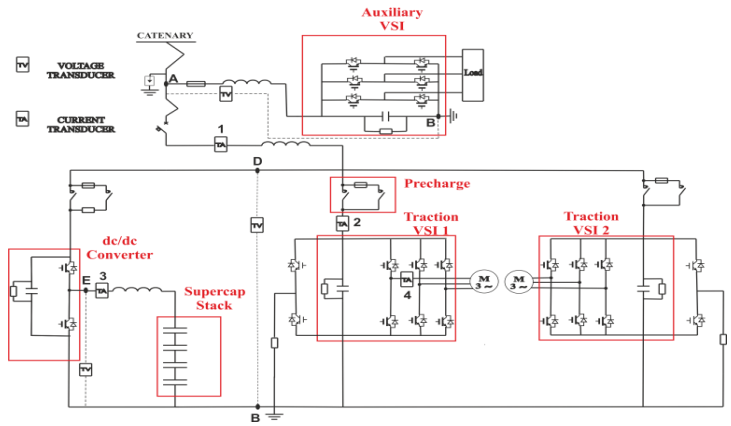

Figure 2.1 **Circuit diagram of a module of the on-board power conversion unit**

During catenary-free operations the energy is given by the supercaps, whose output voltage obviously decreases; therefore the interposed dc/dc converter has to maintain the dc-link voltage within its rated variation range, so that traction and auxiliary systems can be supplied without any problem. The hall effect voltage and current transducers allow an overall monitoring of the conversion system and energy evaluation.

Figure 2.2 depicts the energetic model of the circuit diagram of Fig. 2.1, valid both for traction and braking intervals.

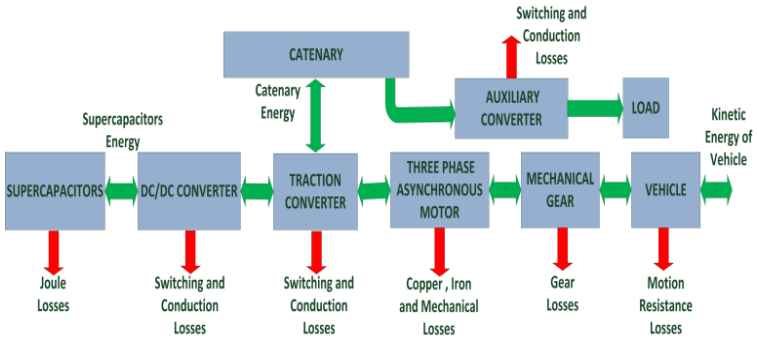

Figure 2.2 **Energetic model of the on-board power conversion system**

Each section of such model has been developed, describing dependence of parameters on dynamic variables.

Supercaps losses depend on the square of the current because they are due to joule losses on the internal resistance (see Figure1.5). Losses in the dc/dc converter are linked to both current and switching frequency of IGBTs. Traction inverter is controlled by means of a PWM technique with variable switching frequency in correspondence of different motor speeds; therefore, inverter and motor losses mainly depend on current and vehicle speed values. Mechanical gear losses depend on friction phenomena between the gear wheels and increase when the speed values increase. Vehicle motion is mainly opposed by rolling resistance and aerodynamic drag.

During catenary-free operations, in the different sub-systems of the power unit in Fig. 2.1 the losses are different from the rated ones, because very low values of cruise speed are accepted in order to make easier to overcome autonomously a certain distance.

2.1.2 Experimental evaluation of on-board Energy Losses

Several experimental tests have been carried out on an experimental tram vehicle with the aim to evaluate power and energy losses in the different sub-systems of an on-board power unit (as in Figure 2.1) during free-catenary operations. The main data and ratings of the considered vehicle are synthesized in Table 2.1.

TABLE 2.1 **Main data of the tested experimental tram vehicle**

Vehicle		***Supercaps stack***		***Traction units***		***Auxiliary units***	
N. of wagons	5	N. of modules in series	4	N. of inverters	4	N. of inverters	2
		Data of each module					
Length [*m*]	32	Ratedvoltage [*V*]	125	N. of motors	4	VSI switching frequency [*kHz*]	2
Weight (empty vehicle) [*ton*]	39	Capacitance [*F*]	63	Type of motors	IM	Rated power of each inverter [*kVA*]	30
Wheel arrangement	B02B0	Energy [*Wh*]	102	Rated power of each motor [*kW*]	105	Power devices	IGBT
Cruise speed [*km/h*]	70	Weight [*kg*]	59.5	VSI switching frequency [*kHz*]	1		
Catenary DC Voltage [*V*]	750	Volume [m^3]	0.086	Power devices	IGBT		

The tests were carried out on an empty vehicle moving along a straight track with a slope of about 1%. Different motion conditions were considered; in the following Fig.s 2.4÷2.9 the time behaviors of some experimentally detected quantities are shown with reference to the speed and traction torque vs time

diagrams of Fig. 2.3., which highlight different operative and motion conditions of the vehicle for a significant test. The vehicle is standstill until $t=t_1$; in the interval (t_0, t_1) it is connected to the catenary in order to charge the supercaps; an accelerating interval of about 20 *s* until t_2 with almost constant acceleration is followed by a short interval (t_2, t_3) with speed around 15 *km/h* and by an interval (t_3, t_4) of about 45 *s* with quasi-uniform deceleration through coasting. The maximum speed of about 15 *km/h* is considered an acceptable target for catenary-free operations in city center paths.

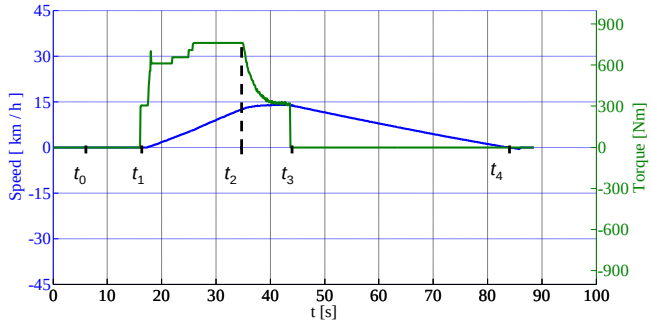

Figure 2.3 **Speed & traction torque vs time in the experimental tests**

Obviously, after lowering the pantograph at $t=t_1$, vehicle traction and on-board auxiliary services are allowed by the supercapacitors system until its voltage reaches the minimum operation value. In particular, the experimental tests discussed in Fig.s 2.4÷2.9 were carried out by operating only one traction VSI and the correspondent induction motor.

Fig.s 2.4 and 2.5 show the time behavior of some voltages and currents detected by TV and TA transducers in Fig. 2.1. In particular, the supercapacitors voltage v_{EB} (red line in Fig. 2.4) lightly increases from t_0 to $t_1 \approx 16$ *s*; after starting the vehicle, v_{EB} decreases until 400V at t≈35s, where in this time period the duty

cycle of the boost converter is kept constant by the control at value of about 1.5 and then also v_{DB} decrease with the same law. After that, the control works in order to sustain the minimum voltage required at dc-link by the traction unit and the voltage v_{EB} decrease until 260 V at $t_3 \approx 44$ s and then remains constant. The correspondent current i_{TA3} (see Fig.2.5) is negative in (t_0, t_1), due to some auxiliary loads and the charging of supercaps from the catenary; it increases until t_3 and becomes 0 after t_3, when the electromagnetic torque developed by the motor is 0. Thanks to the dc-dc boost converter in Fig. 2.1, the v_{DB} voltage (green line in Fig. 2.4) is higher than v_{EB} until t_3, while decreases versus 0 after t_3. Similar values are achieved by the main voltage v_{AB}(blue line in Fig.2.4).

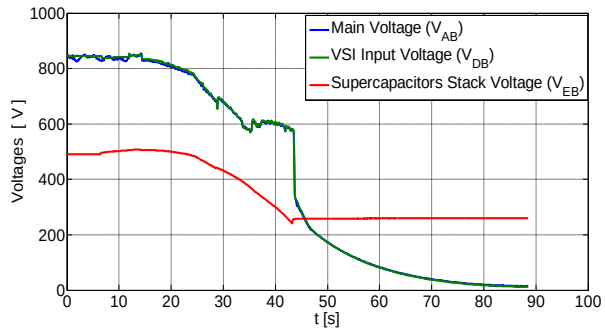

Figure 2.4 **Experimentally detected voltages vs time**

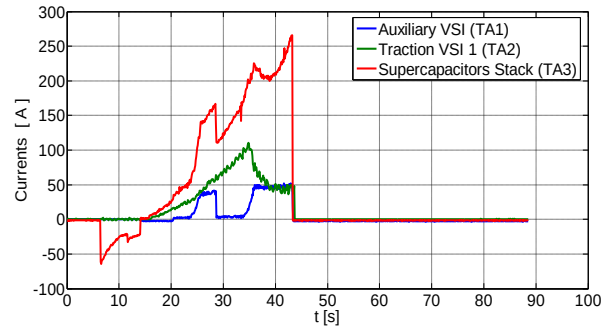

Figure 2.5 **Experimentally detected currents vs time**

The quantities v_{AB} and v_{DB} are the dc-link voltages of the auxiliary and the traction inverters respectively; the control tries to maintain these values $\geq 600\ V$.

From Figure 2.5 we can also observe the behavior of the current i_{TA2} absorbed by the traction VSI and of i_{TA1} requested by the auxiliary loads, which justifies the irregular behavior of the total current i_{TA3} generated by the supercaps stack. Due to the position of the current transducer TA1 in the circuit (Fig. 2.1), in the interval $(0, t_1)$ the blue line of Fig. 2.5 represents the current i_{TA1} absorbed by the catenary and used to charge supercaps, before lowering pantograph.

The time behaviors of losses and energies in the different sections of the on-board power circuit are drawn in Figs. 2.6 and 2.7. In particular, blue and green lines in Fig. 2.6*a* represent respectively the internal losses of the whole supercaps stack (P_{SC}) and of the DC/DC converter (P_{ch}). Both losses are different from 0 only in the interval (t_1, t_3), i.e. during the traction interval in free-catenary operation and are easily evaluated as:

$$P_{SC} = R_{SC}\ i_{TA3}^2 \qquad (2.1)$$

$$P_{Ch} = v_{EB}\, i_{TA3} - v_{DB}\, i_{TA3}\, \delta \qquad (2.2)$$

where R_{SC} is the series internal resistance of the supercaps stack ($R_{SC} = 0.072\ \Omega$) and δ is the chopper duty-cycle. The power of the auxiliary loads (red line in Fig. 2.6*a*) is given by:

$$P_{aux} = v_{AB}\ i_{TA1} \qquad (2.3)$$

This last expression is also used to evaluate the power derived from the catenary during the supercap charging interval ($t_0 \rightarrow t_1$, light-blue line in Fig. 2.6*a*).

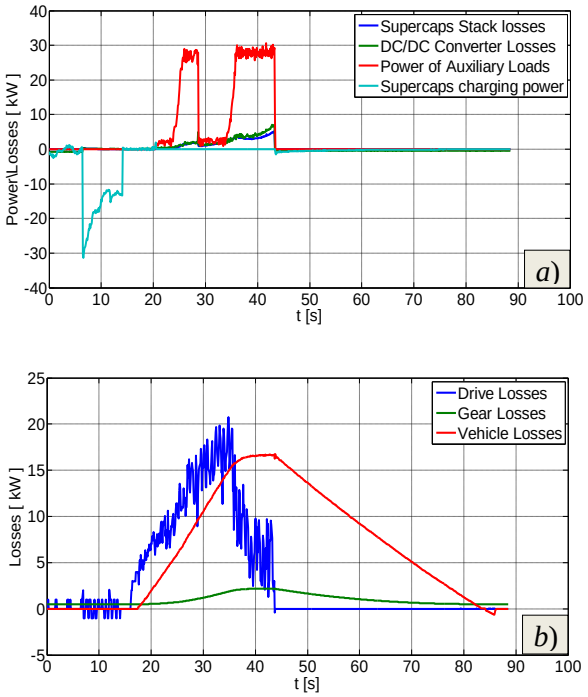

Figure 2.6 **Experimentally detected power and losses vs time**

The losses in Fig. 2.6*b* are indicated in the key-list on the top of the diagram. The blue-line curve represents the losses P_{Dr} in the traction drive (traction converter + induction motor), with:

$$P_{Dr} = n\left(v_{DB}\ i_{TA2} - T_e^*\ \omega_r\right) \qquad (2.4)$$

Where ω_r is the motor angular speed and T_e^* the reference electromagnetic torque. Moreover, n (the number of active traction unit) is equal to 1 for the cases discussed in this section. The losses in the VSI traction converter can be separated from the ones in the motor, by suitably using the values of the motor electrical parameters and the conduction and switching losses of the VSI power devices.

The gear losses P_{Ge} (line green in Fig.2.6*b*) are evaluated as:

$$P_{Ge} = a + b\, v_{Tr}^2 \qquad (2.5)$$

where v_{Tr} is the measured speed of the tram in *km*/*h*, while the coefficients *a* and *b* have been evaluated by means of specific tests executed by gear manufacturer. The vehicle friction losses are evaluated when the motion of vehicle is by inertia, i.e. T_e^*=0, as:

$$P_{Fr} = R_{mot}\frac{v_{Tr}}{3.6} = \left(\rho G + \lambda\, v_{Tr}^2 + \gamma\, g\, G\right)\frac{v_{Tr}}{3.6} \qquad (2.6)$$

where R_{mot} is the total motion resistance, *G* the weight of the vehicle in *ton*, *g* the gravity acceleration (9.81 $m\ s^{-2}$), γ the slope in ‰ (10‰ in the considered case), v_{Tr} the speed in *km*/*h*, ρ and λ are resistance coefficients dependent on vehicle, wheel and track. The instantaneous values of the power in different points of the circuits are comparatively shown in Fig. 2.7 during the charging of supercaps and autonomous (catenary-free) operations. The peak value of the power generated by the supercaps is about 80 *kW*, while the maximum power available at the motor shaft is about 40 *kW*, due to the significant values of both losses and power requested by the auxiliary services.

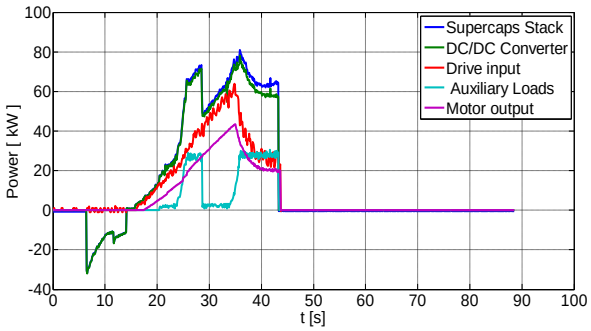

Figure 2.7 **Power in the different sections of the vehicle**

By handling the acquired data shown in the Fig.s 2.6 &2.7, the energy vs time curves of Fig. 2.8 can be obtained.

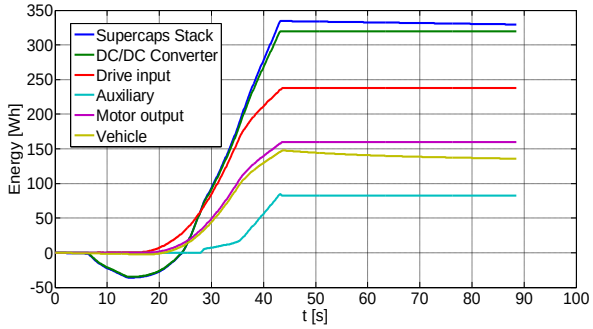

Figure 2.8 **Energy vs time for each section of the vehicle**

They represent the cumulated values of the requested energy in the different sections of the power conversion system of the vehicle, mainly during catenary-disconnected operations.

The behavior of the motion resistance R_{mot}/G (expressed in N/ton) is plotted vs. vehicle speed in Fig. 2.9, where the experimental values are fitted by a second order polynomial curve.

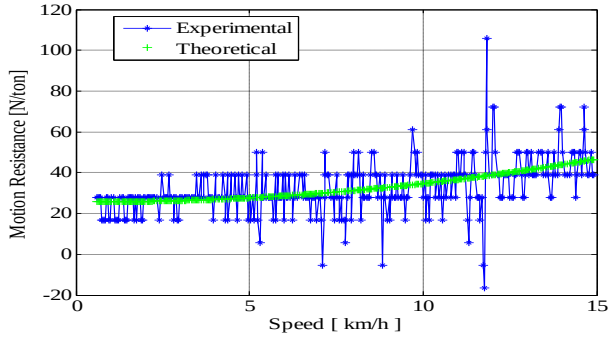

Figure 2.9 **Experimental motion resistance R_{mot}/G (blue line) and polynomial curve fitting (green line).**

2.1.3 Sizing of the Supercapacitors ESS

As already mentioned, the measurements described in §.2.1.2 have been repeated several times, also in different operating conditions, on the experimental tram of Tab. I running also in catenary-free mode. By properly handling the results of this experimental investigation a simple energetic model of the vehicle has been pointed out. This model allows to estimate the energy required by the vehicle to run standalone along various kinds of routes. The energy values refer to straight paths having different slopes and lengths. All considered paths are characterized by a typical trapezoidal profile, with acceleration and deceleration intervals of 0.4 m/s^2 and cruise speeds variables from 10 to 25 *km/h*.

In the simulation analysis the additional weight of the supercapacitor units is taken into account and in Figure 2.10 is depicted the flow chart of the procedure implemented in Matlab. The procedure can be summarized as: I) experimental test sections for a real Tram ; II) energetic model of vehicle and estimation of motion resistance; III) desired speed-time diagram with different slopes, lengths and cruise speeds; IV) evaluation of the amount of energy to carry out the assigned route; V) estimation of the total capacitance needed. The additional weight for the vehicle due to the supercapacitors increase the amount of energy required for the movement of the vehicle if the dynamic performance are fixed.

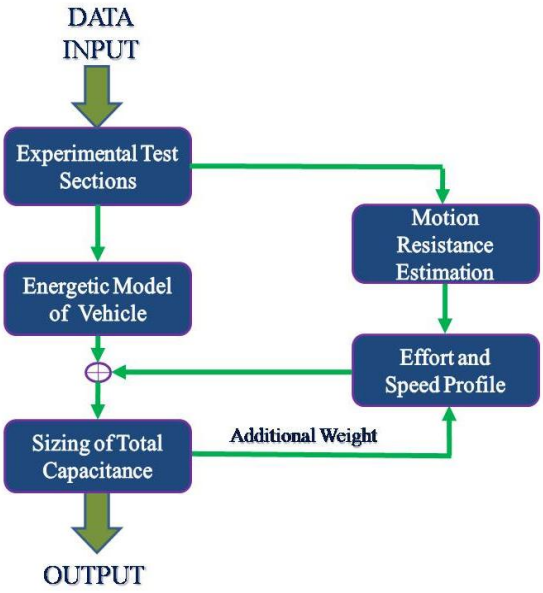

Figure 2.10 **Block diagram of proposed procedure**

Figure 2.11 shows the estimated values of the stored energy (see equations 2.7 and 2.8) for different path lengths and slopes, taking into account different cruise speed for the routes. The required energy increases almost linearly as a function of the length to be covered and the slope of the route in catenary-disconnected mode.

$$W_{Vehicle} = \int_{t_i}^{t_f} F_{Tr}(t) \cdot v_{Tr}(t)\, dt \qquad (2.7)$$

$$W_{SC} = \frac{W_{Vehicle}}{\eta_{SC} \cdot \eta_{Dr} \cdot \eta_{Gear}} \qquad (2.8)$$

The results in Fig. 2.11 can be easily used to end up the procedure “design to range” aimed to estimate the sizes of the supercapacitors needed to properly extend the autonomous operating range of the considered tram.

The evaluation of needed capacitance should take into account that:

- the dc-link rated voltage is 750 *V*;

- the maximum voltage ratio of the dc-dc converter in Fig. 2.1 is about 2.3 (in boost mode);

- each supercapacitor bank (as available on the market) is composed by four series-connected modules (rated voltage 125 *V*), whose main data and ratings are in the second column of Table 2.1.

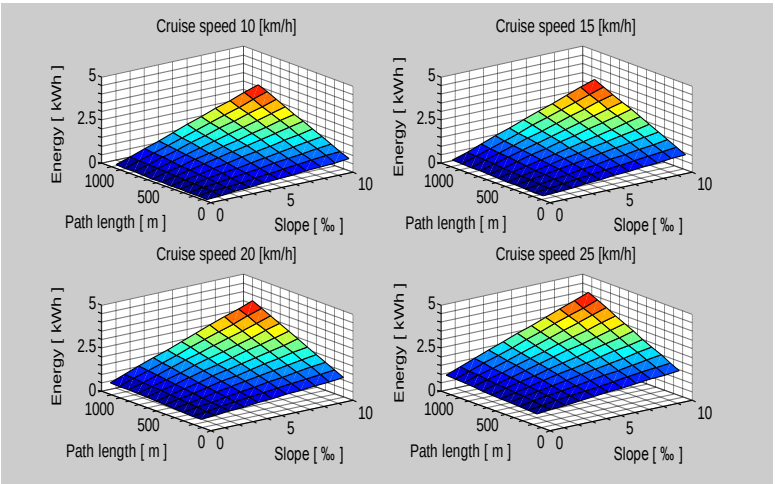

Figure 2.11 **– Stored energy vs. path length vs. slope for different cruise speed in standalone operations**

In Fig.2.12 b) , the total capacitance required to the supercapacitors is plotted as a function of the path length and in Fig.2.12 a) are depicted the corresponding energies needed to perform the route autonomously, taking into account a speed time diagram with same cruise speed of Fig. 2.3.

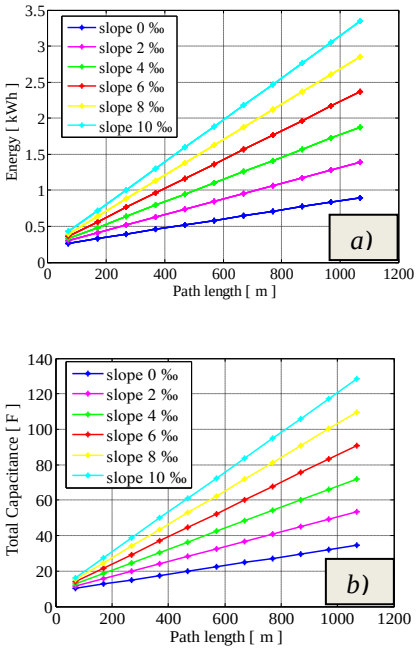

Figure 2.12 **– Design procedure in catenary-free operations for speed-time diagram with cruise speed of 15 *km/h* : a) Stored energy vs. path length; b) Supercapacitors total capacitance vs. path length**

The rated voltage of the supercapacitor bank is 500 V (=4*125 V); its minimum voltage is 250 V. The considered vehicle needs from about 0.25 to 3.4 kWh in order to cover 1100 m with a slope variable from 0 to 10 ‰. For instance, in case of a catenary-free length of about 1100 m with slope 10 ‰, 9 parallel connected banks are needed, with a total weight of about 2.15 *tons* and a volume of about $3.1m^3$.

The results of the proposed methodology seem compatible with the considered vehicle, in terms of values of capacitance, weight and dimensions of supercapacitors, also for more than one thousand meters of autonomous running with lowered pantograph.

2.2 Stationary SESS in Light Railway System

The stationary configuration of SESS consists in the installation of one or several SESS placed along railway tracks. In this way is possible to store a part of braking energy that cannot be directly supplied to other non-receptive vehicles and feed it back into the overhead contact lines for subsequent accelerations in the same electrical supply section. On the other hand, is conceivable believe that the possibility of reduce the voltage drop along the power supply line allows the optimization of supply voltage profile with the benefit in the mid-long term of being able to reduce the costs due to new investment for infrastructure (i.e., avoiding the introduction of new Electrical SubStations (ESs) and / or reducing the section of the cables). Moreover, in the case of Metro systems, the use of SESSs lead to the reduction of thermal effects in gallery due to the dissipation of energy through the braking chopper.

In Figure 2.13 is shown a simplified example of non-receptive light rail network section with the inclusion of stationary SESS. The aim is put in evidence the physical connection of different sub-systems and the possible scenarios of power flows exchanged between them during the motion of the vehicles.

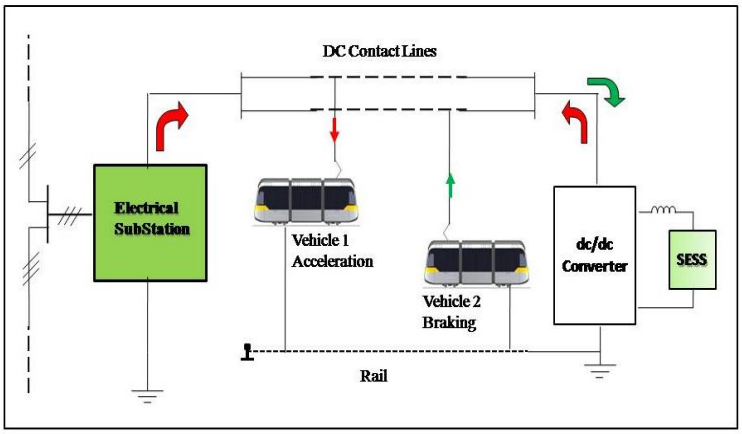

Figure 2.13 **Stationary SESS in Metro network section**

In case of discharge, the energy is directed from SESS to the vehicles with also a contribution of the substation; instead, in the process of charge the energy flow is reversed.

It is important to say that the suitability of stationary SESS for the whole electrified transportation system is strictly connected to their size, position and operating conditions. For the design and placement issue, it is important to take into account the variability of the traffic conditions and the service frequency and in this regard, some optimization procedures based on a nonlinear programming technique have been developed and verified by means of a light-rail system simulation and laboratory tests [33], [56]÷ [59].

From the point of view of the control, the main difficulties are related to the choice of the time periods for storing and providing energy according to the network status which depends mainly on the traffic evolution. In literature has been proposed a power flow controller to handle the energy flow as a function of the state of charge and evaluated the influence of the ESS size and positioning along the line with reference to a simulation on one

metro line in Brussels [33], [56]÷ [61]. Furthermore, a changeover power flow management method has been proposed, based on the definitions of three different states where the transition conditions were based on the defined voltage limits and ESS state of charge ([62] , [63]) . It is worth of remark that in this study only control issue will be addressed.

Due to this concerns, the identification of suitable control strategy for stationary SESS may involve in significant advantages carrying out the optimization of the energy flow among the running vehicles and substations. Hence, the focus of this study is the introduction and validation of a control strategy, able to fulfill the benefits above discussed by means of experimental results obtained by using a prototype of a light rail system.

2.2.1 Configuration of the System

The system depicted in Figure 2.13 represent the baseline for the configuration which deals with integration and management of stationary SESS but in Figure 2.14 is pointed out the electrical diagram of the configuration adopted.

In particular, a model scaled of a light rail system is considered in this study with a rated voltage of 750 V supplied by a single DC electrical non receptive substation located at one terminal and integrated by the presence of SESS at the opposite terminal of the track. The voltage drop is variable with the motion of the vehicle and its maximum is reached at the opposite terminal with respect to the substation.

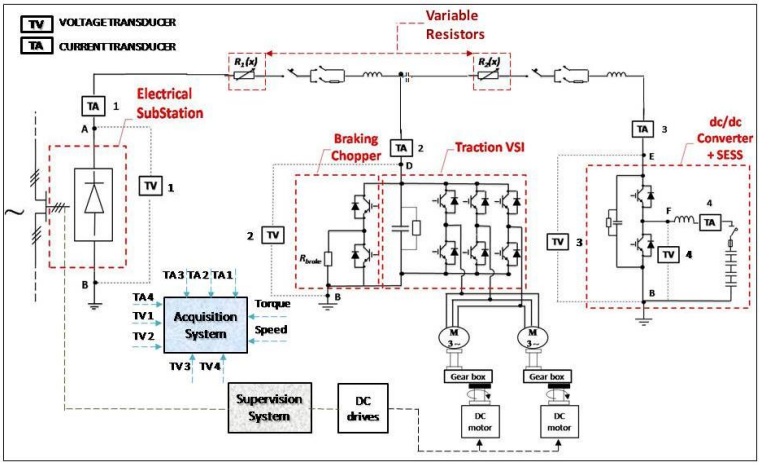

Figure 2.14 **Circuit diagram of the system**

The vehicle is represented by a single propulsion unit of a Metro rail vehicle, where his configuration is made of a 3-ph PWM-VSI feeding two induction motors (IM) in parallel connection, including also the module for the braking chopper. Their behavior is regulated according to the control laws provided by the Traction Control Unit (TCU). The load is simulated through two DC motors coupled to the IMs by means of mechanical gears and controlled by a Supervision System.

The movement of the vehicle along the line is schematically represented by means of a variable rheostat with center tap which is used to simulate the variation of the electrical resistance of the line both for Electrical Substation and SESS with reference to the position of vehicle. These resistance are indicated, respectively, with R_1 (x) and R_2 (x), where "x" indicate the vehicle position and relative values are interrelated by relations:

$$\begin{cases} R_1(x) = R_2(l_{tot} - x) \\ R_{tot} = R_1(x) + R_2(l_{tot} - x) \end{cases} \qquad (2.9)$$

A dc-dc converter is used as interface of SESS stack versus the dc-link and Supercapacitor Control Unit (SCU) allows the switching of their IGBTs, according to the control law implemented for this study. SESS stack is made of 4 modules connected in series, each one having a rated voltage of 125 V and capacitance of 63 F with feasible amount of energy stored of about 136 Wh.

The energy available in this configuration for SESS stack is about 75% of the total value, because they may reach not less than the half value of rated voltage in discharging phase and no more than the rated value in charging phase, as a result, respectively, of the constraints on the operating conditions of dc/dc converter and the minimum value of voltage for dc-link.

Electrical and mechanical quantities of interest are acquired from the transducers by the Acquisition System as pointed out in Figure 2.14. Four current and voltage transducers Hall effect have been adopted for electrical quantities, while speed and torque transducers have been used for speed and the torque applied to the axles.

2.2.2 Control Strategy

The performance in terms of the energy saving, power peak shaving and voltage profile optimization depend on how energy flow is managed. In Figure 2.15 is depicted a generic overview of voltage levels used by the control to select the status of dc/dc

converter.

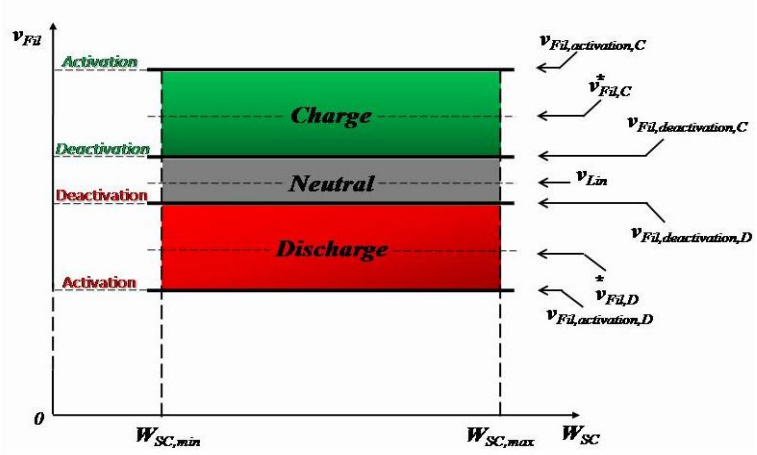

Figure 2.15 **States management of dc/dc converter**

The measurement of voltage at the dc-link terminals of dc/dc converter, gives the information about the electrical evolution of the network which depends mainly by the motion phases of the vehicle/s (i.e. acceleration, cruising, braking or coasting).

As shown in Figure 2.15, the possible states of the dc-dc converter are individuated in three different working areas, that is *charge*, *discharge* and *neutral* where they are delimited between minimum / maximum values of energy for SESS and activation / deactivation thresholds on the voltage. It is also important to say that the currents of SESS are severally positive (charge) and negative (discharge) according to the convention adopted for TA 4 (see Figure 2.14).

In particular the references and thresholds of the voltage may be settable and the choice of their values, in general, depends on the position in which SESS are allocated with respect to the electrical substation and traffic evolution, or in other words, in the knowledge of daily voltage profile in that point.

In Figure 2.16 is pointed out the control scheme of dc/dc converter adopted for the operation of SESS.

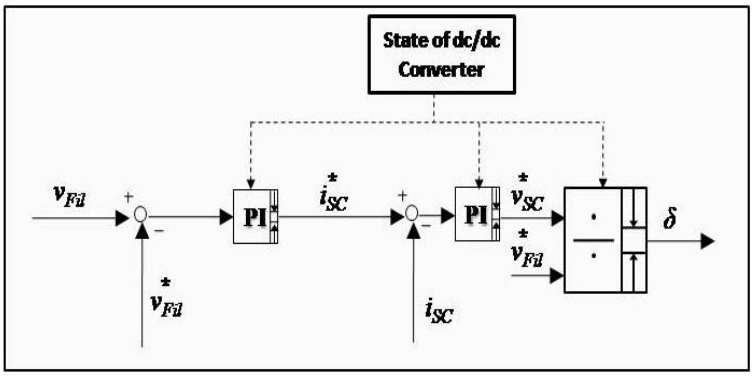

Figure 2.16 **Control block diagram for Stationary SESS**

Two cascade control loops have been developed; a control loop on the dc-link voltage of dc/dc converter carried out by means of a standard PI which produce the desired value of current for SESS :

$$\overset{*}{i}_{SC} = k_{P,V}\,(v_{Fil} - \overset{*}{v}_{Fil}) + k_{I,V}\int_0^t (v_{Fil} - \overset{*}{v}_{Fil})\,dt \qquad (2.10)$$

Another control loop on the charge / discharge currents, also in this case using a PI regulator, to provide the duty-cycle for the IGBTs of the converter :

$$\overset{*}{v}_{SC} = k_{P,i}\,(\overset{*}{i}_{SC} - i_{SC}) + k_{I,i}\int_0^t (\overset{*}{i}_{SC} - i_{SC})\,dt \qquad (2.11)$$

The synthesis of the controllers is the standard procedure of cascade control structure design ([64],[65]). The first step is the synthesis of the SESS current controller while the second step is the synthesis of the SESS voltage controller. The controllers are conventional PI because first-order systems have to be controlled

and time constant of the external loop is chosen to be ten times higher than the internal loop ([66],[67]). In this way, the controllers have been designed by the classical pole placement method to decouple the two control loops. However, a further experimental setting of the control parameters it has been necessary in order to deal with satisfactory behaviour in dynamic and steady conditions.

2.2.3 Experimental Results

In the test room of Hitachi Rail Italy has been set up the demonstrator circuit represented in Figure 2.14, and the section related to the stationary SESS is shown in Figure 2.17 where the numeration indicates: 1) SESS stack; 2) dc/dc converter; 3) variable rheostat; otherwise, in Table 2.2 are summarized the main data of the whole demo circuit.

Figure 2.17 **Section of demo circuit**

TABLE 2.2 **Main data of the Demonstrator**

Electrical Substation		***Supercapacitors stack***		***Propulsion unit***		***Rheostat***	
Max Voltage [V]	4000	N. of modules in series	4	N. of inverters	1	Total resistance [Ω]	0.6
		Data of eachmodule					
Max peak Power [MW]	16	Ratedvoltage [*V*]	125	N. of motors	2	Step resistance [Ω]	0.06
Max peak Current [A]	1000	Capacitance [*F*]	63	Type of motors	IM	N. of contactors	10
Catenary DC Voltage [*V*]	750	Energy [*Wh*]	136	Rated power of each motor [*kW*]	145	Max Current [A]	250
		Weight [*kg*]	59.5	VSI switchingfrequency [*kHz*]	1		
		Volume [m^3]	0.086	Power devices	IGBT		

Several tests have been carried out considering a standard speed-time diagram usually performed in light railway vehicles such as, acceleration cruising, coasting and braking phases, choosing the values of torque delivered on the axles according to the maximum current that contactors of variable rheostat may lead.

A fine-tuned analysis has allowed the choice of voltage references and thresholds which optimizes the operations of the whole system. Table 2.3 arranges the settings adopted for two configuration in the test room most significant in terms of *energy saving*, *voltage profile optimization* and *power peak shaving*.

TABLE 2.3 **Test room configurations**

Test	V_{Lin}	$V^{*}_{Fil,C}$	$V^{*}_{Fil,D}$	$V_{Fil,activation,C}$	$V_{Fil,deactivation,C}$	$V_{Fil,deactivation,D}$	$V_{Fil,activation,D}$	R_1	R_2	SESS
I	750V	770V	740 V	800 V	760 V	750V	730 V	0,6 Ω	0 Ω	NO
II	750V	770V	740 V	800 V	760 V	750V	730 V	0,6 Ω	0 Ω	YES

Two configurations, one with the presence of SESS and another keeping disconnect the storage system have been pointed out. In both cases, the voltage of ES is about 750V and the initial values of the resistances, show that the movement of vehicle is simulated from SESS to ES.

In Figure 2.18 are depicted Torque and Speed profiles of the propulsion unit. A typical trapezoidal speed time diagram has been considered with acceleration and deceleration equal to *0.4* m/s^2 and cruising speed value of about *43 km/h.*

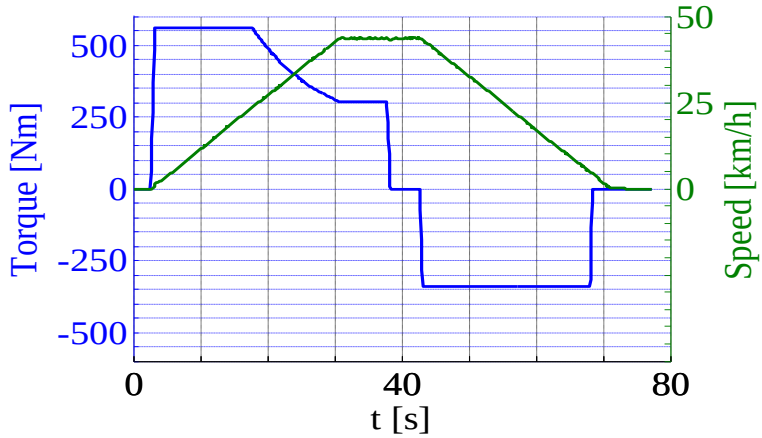

Figure 2.18 **Experimentally Torque and Speed time diagrams**

Fig.s 2.19 & 2.20 depict for Test I, where SESS is switched off, the time operations of the electrical quantities referred to the torque and speed-time diagrams of Figure 2.18.

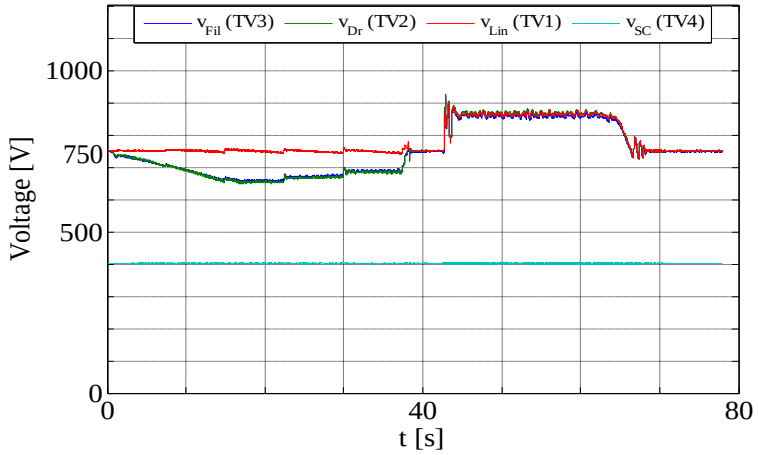

Figure 2.19 **Test I : Experimentally detected voltages vs time**

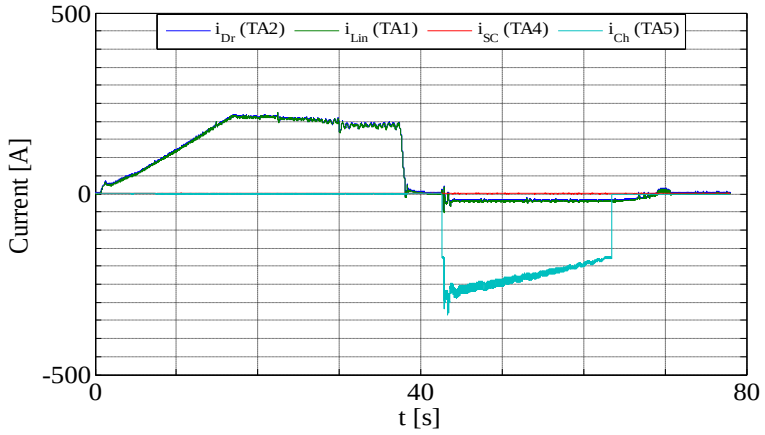

Figure 2.20 **Test I : Experimentally detected currents vs time**

The voltages of ES (TV1), input drive of propulsion unit (TV2), input of dc/dc converter (TV3) and SESS (TV4) are displayed in Figure 2.19. In acceleration, the voltage drop due to the motion of vehicle reach its maximum value of

$\Delta V_{Dr}^{\max} = 100V$ at t = 20s, while in braking the time behavior of the voltages are almost equal. The voltage of SESS stack is steadily equal to *400 V* because they are not operated in this situation. Instead the current of ES (TA1), propulsion unit (TA2), SESS (TA4) and braking chopper (TA5) are illustrated in Figure 2.20. The max value of the current provided by the ES $i_{Lin}^{\max}$ is about 223 A at t = 23.4 s corresponding to the cruising phase. As expected, the current of SESS is equal to zero so the power line provide all the energy needed for the propulsion unit. The time behavior of braking chopper current is described by the average time diagram, i.e. time values acquired from TA5 multiplied for duty cycle. By analyzing the operations of braking chopper, it works first as "spillway" avoiding that the overvoltage at input drive during the braking transient assume values which may lead to the fault for the filter capacitor. Moreover, the control of the braking chopper allows to keep the voltage at eligible values dissipating the power in surplus.

In Fig.s 2.21 & 2.22 are depicted the same electrical quantities as in Fig.s 2.19 and 2.20 for the case in which the SESS is involved (test II), related always to the mechanical quantities of Figure 2.18.

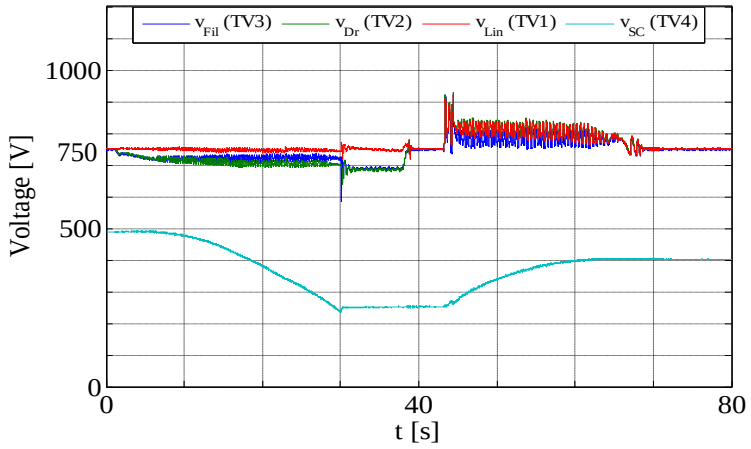

Figure 2.21 **Test II : Experimentally detected voltages vs time**

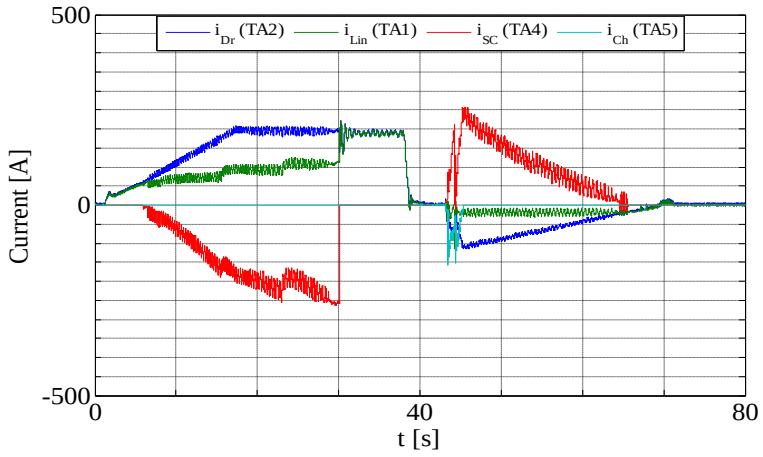

Figure 2.22 **Test II : Experimentally detected currents vs time**

Looking at Figure 2.21, the SESS has been previously charged at voltage value of about $v_{SC} = 495V$. In motion phases briefly described as "traction" (acceleration + cruising), the control works to sustain the line current (green line Fig. 2.22) through the SESS current (red line Fig.2.22), keeping the voltage (blue line Fig. 2.21) close to the reference value of *740 V* until the storage system provide all the available energy bringing his

voltage to the value $v_{SC} = 255V$ at t = 30 s. Instead, during the braking phase the operations of braking chopper involve only the "spillway" functionality (cyan line Fig. 2.22) as previously described while Supercapacitors store the energy differently dissipated. The control manages with the charge of SESS holding the value of dc-link voltage of dc/dc converter (blue line Fig. 2.21) near the reference value of 770V.

In Table 2.4 are evaluated the energy in traction and braking phases, with reference to each subsystem of interest.

TABLE 2.4 **Energetical evaluations from experimental Test sections**

	Test I		***Test II***	
Energy	Traction	Braking	Traction	Braking
W_{Lin} [*Wh*]	1230.5	-104.2	793.2	-101.2
W_{Drive} [*Wh*]	1121.7	-328.7	1119.6	-328.7
W_{SC} [*Wh*]	0	0	-391.3	214.5
W_{Ch} [*Wh*]	0	216.4	0	4.9

It is clear that looking at energy provided from ES during traction phase, the SESS supports the power line using the energy previously stored to sustain the propulsion unit and the losses of the line. In braking, SESS allows the recovering of a large amount of the energy regenerated in line by limiting the operations of the braking chopper.

In terms of peak shaving, by comparing the line currents in Fig.s 2.20 and 2.22 (see green lines) looking at t = 23.4 s, the reduction of peak current is about *42%* .

The line voltage drop smoothing action carried out by the stationary SESS is clearly highlighted in Figure 2.21 which displays the voltages of both supply line (v_{Lin}) and input drive(v_{Dr}). At t = 20s, the maximum voltage drop is in this case about $\Delta V_{Dr}^{\max} = 42V$, with a reduction of *58%* with reference to the test I. Moreover, the management of voltage profile imply the reduction of the losses on the feeding line during traction phase of about *60%*.

Chapter 3

Energy saving and Sensorless control for IM and PM-brushless drives in LRT Systems

In the technical literature a very large number of methods were proposed for speed sensorless of IM or PMSM drives (see for example [69], [72]÷[73]); however an efficient speed estimation on the whole operation range with a suitable robustness/immunity to noise and to variations of machine parameters is not yet completely obtained. In order to overcome these problems and taking into account the typical control requirements of railway traction field in speed-sensorless applications ([75],[82],[83]), some authors have separately addressed the issues occurring in the different operating conditions.

In this chapter, two different traction architectures of a light railway vehicles with IM or PM brushless motor drives are investigated by means of two kind of speed-sensorless field-oriented vector control. The dynamic and energy performance of propulsion units with IM and PMSM drives are evaluated and compared in correspondence of various operating conditions of railway traction vehicle over the entire speed domain. Moreover, taking into account typical profiles of urban routes, some well-known typical problems of speed-sensorless control have been addressed such as in correspondence of uphill starts of railway vehicles or in the so-called re-powering mode, just after an interval in which the motor is switched off for "coasting", to carry out improvements in terms of reliability and energy efficiency for the whole railway system.

3.1 Configurations of the Vehicle equipped with IM or PMSM drives

Usually urban railway vehicles are required to carry out a path consisting in *acceleration*, *cruise*, *coasting* and *braking* phases (many times a day). Since in urban services the distance between two consecutive stops is relatively small, acceleration and deceleration phases are relevant in comparison with the cruise region, which is shorter than in cases of medium-long distance trains.

For the railway vehicle considered in the following sections, the propulsion units are assumed with the two different configurations of Fig.3.1 and Fig.3.2 . In addition , the main characteristics of the vehicle are summarized in Table 3.1.

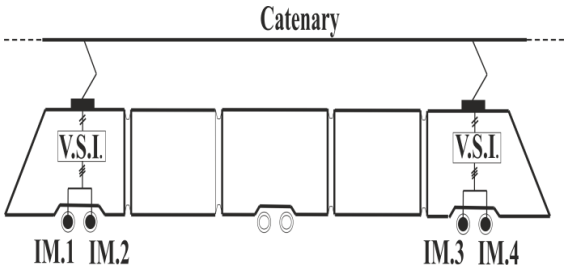

Figure 3.1 **Vehicle configuration with an IM propulsion drive.**

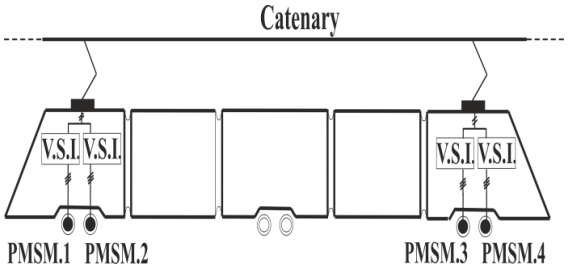

Figure 3.2 **Vehicle configuration with a PM brushless propulsion drive.**

TABLE 3.1 **Vehicle main data**

Total Mass (empty ÷ full)	52÷68	*tons*
Maximum Acceleration	1.1	m/s^2
Maximum Deceleration	1.1	m/s^2
Maximum Speed	80	*km/h*
Wheel Diameter	0.68	*m*
Mechanical Gear Ratio	5.5	
Mechanical Gear	0.95	

The vehicle presents five wagons, with a total length of about 32*m* and a running gear B02B0. For the vehicle equipped with an IM drive, the whole power is divided in 2 traction units, each with 2 IMs; single-inverter dual-motor is the architecture of each propulsion unit. On the contrary, in the case of PM brushless drive, four dedicated inverters are used, because synchronous machines cannot be operated in parallel connection for traction applications.

Main rated data of the considered IM and PMSM propulsion units are synthesized in Table 3.2.

TABLE 3.2 **Data of the traction units**

	IM	PMSM	
Rated motor power	127.6	127.5	*kW*
Rated electromagnetic torque	647	812	*Nm*
Rated motor speed	1884	1500	*Rpm*
Motor pole-pair number	2	4	
Rated armature voltage	443	285	*V*(*rms*)
Rated armature Current	230	314	*A*(*rms*)
Inverter power switches	CM1800HCB34N	CMH1200DC34S	
Inverter switching frequency	1000	2000	*Hz*
Catenary dc voltage	750	750	*V*

The main parts of a traction units are shown more in detail in Fig.3.3 and 3.4; as already mentioned, only for IM

drives two motors are supplied by only one VSI while for PMSM drives, each motor is feeded by his own converter because of skidding phenomena between the different axles which may affect the position control. The IGBT modules selected for the VSI are different for the two examined drives with IM or PM brushless (see codes of inverter power switches in Tab.3.2).

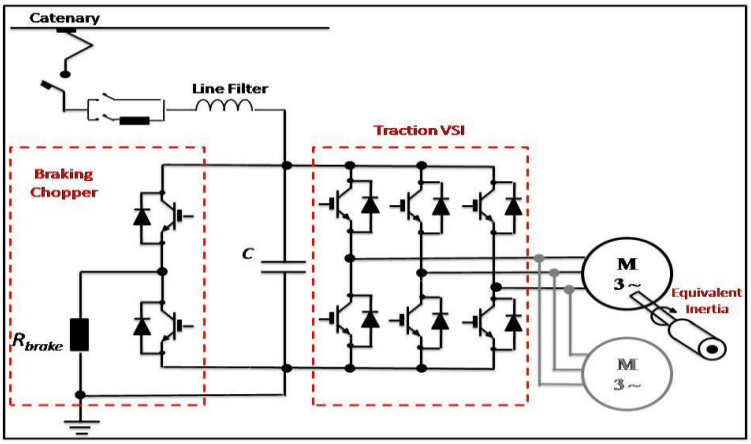

Figure 3.3 **Schematic electrical diagram of a IM traction unit.**

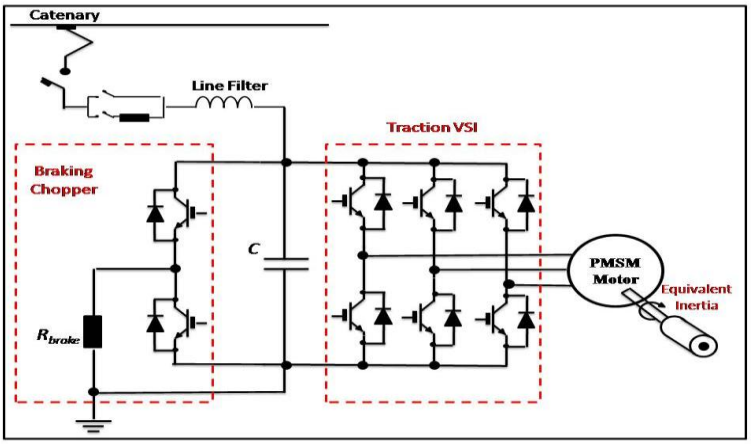

Figure 3.4 **Schematic electrical diagram of a PMSM traction unit.**

In Table 3.3 are indicated the parameters of the traction motors considered for the propulsion units.

TABLE 3.3 **Parameter Configurations**

Parameter	IM	PMSM	
R_s	0.01816	0.014	Ω
L_s	5.3	0.434	*mH*
L_m	5.1		*mH*
L_r'	5.4		*mH*
R_r'	0.01458		Ω

3.2 Sensorless Control in Railway Applications

The utility to remove speed or position sensor is usually linked to different reasons as cost, cabling simplicity, robustness and construction constraints. For these reasons, the use of sensorless control strategy in IM or PMSM traction drives makes possible to improve reliability, reduce maintenance and increase motor rated power, taking advantage by the space usually reserved to speed and position sensors and their accessories. Many different sensorless control strategies are commonly used in IM and PMSM drives and the most utilized in literature are reported in Fig.3.5, where the usual terminology is used. Moreover, Table 3.4 synthetically compares some features of different sensorless techniques, with reference to the motor mathematical model based on the fundamental of the air-gap flux-density distribution [69] ÷ [83].

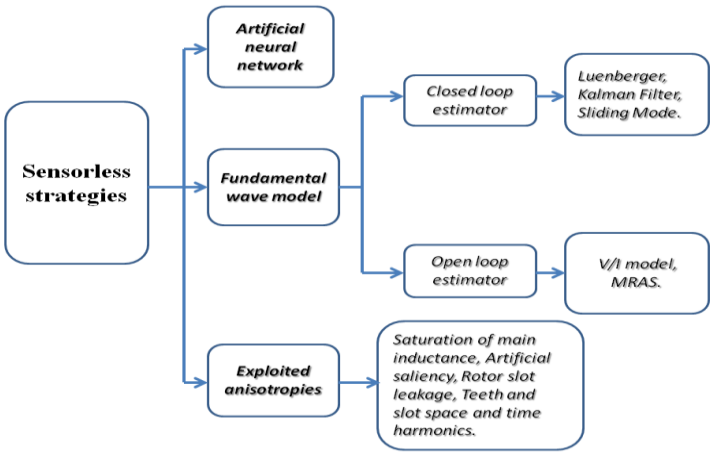

Figure 3.5 **Methods for estimations in sensorless control**

The methods that do not require high performance are essentially based on the steady-state model of the machine. These methods are easy to implement in hardware structures of limited resources. They also have the advantage of not depending too much by the machine parameters. Conversely they have slow responses to transients.

There are schemes that have excellent performance even in open loop. They are based on the dynamic model and knowledge (direct or indirect) of voltages and stator currents. Their operations in open loop implies that their behavior definitely depends on the parameters of the machine. The non-linearity present in the system and the non-perfect knowledge of the values of the parameters during the transient invalidate the performance of such estimators especially at low speed.

Otherwise, the performance of closed-loop observers are slightly dependent on the machine parameter variations far from low-speed region. Sliding mode refers to a control system with variable structure for feedback of state, changing the behavior of

a nonlinear system through a control signal in high frequency. Such control is robust and versatile and also in low speed region good behavior is guaranteed, despite the parameter variation. In some cases (e. g. Kalman filter), good immunity to noisy signals is also ensured. However, some main drawbacks are: -difficulty in gain tuning; -high computational complexity; -difficulty remains in state-observation at low speed values.

However, the hardware control platforms of railway vehicles could have power calculation not fairly to include closed-loop observers. This is due to the standardization of vehicle macro-components, which frequently have life duration of several decades and, then, microcontrollers of old generation may still be on-board. Furthermore, most of these methods require the measure of all the currents and voltages at the inverter terminals, while in the railway context only the dc-link voltage and two currents are usually measured in order to minimize the number of sensors.

TABLE 3.4 **Comparison of sensorless control strategies**

	Suitability in Railway Field			Power Calculation Needed			Number of Control Parameters			Sensitivity to Machine Parameters		
	High	*Medium*	*Low*	*High*	*Medium*	*Low*	*High*	*Medium*	*Low*	*High*	*Medium*	*Low*
Open Loop	x					x		x		x		
M.R.A.S.		x			x			x			x	
Luenberger Observer		x		x			x					x
Kalman Filter		x		x			x					x
Sliding Mode Observer			x	x			x					x

For these reasons, at the present, the use of simple estimators seems compatible with speed-sensorless railway applications, despite their sensitivity to machine parameters variations and the performance decay in low-speed region.

However, the control has to satisfy the specific performance of railway traction drives as:

- operation in the complete motion diagram (following traction torque profile);
- control in re-powering conditions;
- vehicle starting from uphill conditions.

3.3 Sensorless strategy for IM unit

In the following we refer to a speed estimation algorithm based on the well-known model of induction motors in *d-q* rotating reference frame.

With reference to the control diagram of Fig.3.6, the estimated speed value $\hat{\omega}_r$ is deduced from the reference slip angular frequency ω_σ^* and from the instantaneous angular frequency $\hat{\omega} = \mathrm{d}\hat{\psi}/\mathrm{d}t$ estimated by means of the equation:

$$\hat{\omega} = \frac{\mathrm{d}\hat{\psi}}{\mathrm{d}t} = \frac{L_r'}{L_m}\left[\frac{e_{rq}}{\Phi_r^*} - \left(k_{P,c}\, e_{rd} + k_{I,c}\int_0^t e_{rd}\,\mathrm{d}t\right)\right] \quad (3.1)$$

where:

- $\hat{\psi}$ is the estimated instantaneous angular position of the rotor-flux in the stationary α, β armature frame;

- $L_r' = L_m + L_{\sigma r}'$ is the total rotor inductance referred to the stator;

- Φ_r^* is the magnitude of the space-vector of the reference air-gap rotor-flux;

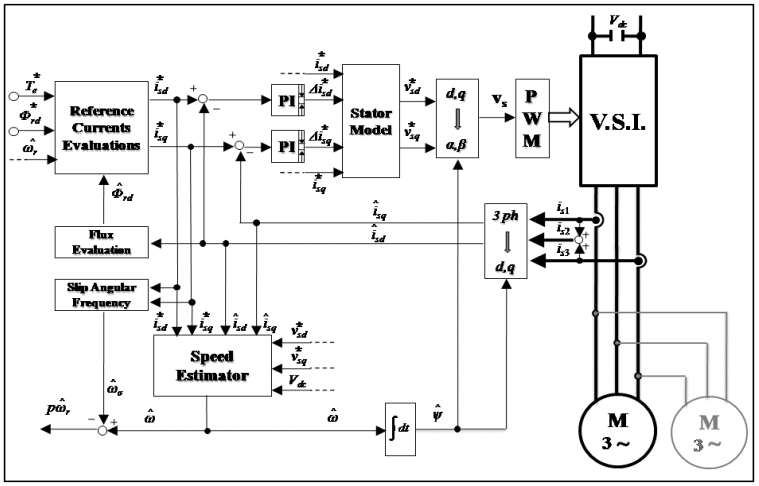

Figure 3.6 **Block diagram of speed sensorless control in IM traction drive.**

In the eq.(3.1) the quantities e_{rd} , e_{rq} are the *d, q* components of the e.m.f. induced in the stator phase by the air-gap rotor-flux and evaluated by means of ([84]):

$$\begin{aligned} e_{rd} &= v_{sd}^{*} - R_s\, i_{sd} - \sigma_s L_s \frac{\mathrm{d}\, i_{sd}}{\mathrm{d}\, t} + \omega\, \sigma_s\, L_s\, i_{sq} \\ e_{rq} &= v_{sq}^{*} - R_s\, i_{sq}^{*} - \sigma_s L_s \frac{\mathrm{d}\, i_{sq}^{*}}{\mathrm{d}\, t} - \omega\, \sigma_s\, L_s\, i_{sd}^{*} \end{aligned} \qquad (3.2)$$

with:

- $L_s = L_m + L_{\sigma s}$ is the total stator inductance;

- $\sigma_s = 1 - L_m^2 / L_s\, L_r^{'}$ is a dimensionless coefficient;

The compensation term in round parentheses of eq.(3.1) aims to nullify the deviation of the rotor-flux angular position ψ from the reference one ψ^{*} (see Fig.3.7). This can occur in transient operations and considerably influences the e_{rd} values.

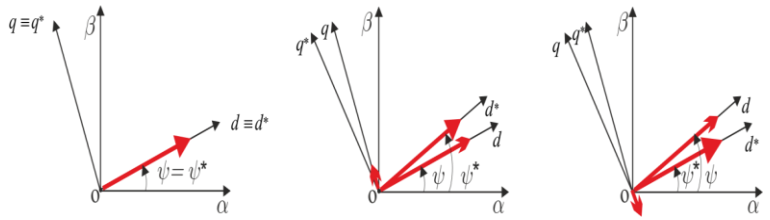

Figure 3.7 **Possible positions in the α, β stator frame of actual and reference rotor flux space-vectors**

The diagram of Fig.3.6 is an indirect field-oriented torque control scheme, where T_e^* is the reference electromagnetic torque and $p\hat{\omega}_r$ the estimated speed in electrical degrees (p is the pole-pair number). The reference value of the air-gap rotor-flux magnitude Φ_r^* is kept constant within the base-speed value; after that value, the flux is decreased at constant armature voltage.

The evaluation of the limit values of i_{sd}^*, i_{sq}^* currents is made off-line and the results are placed in a look-up table, as shown in equations (3.3) :

$$\begin{cases} i_{sd,L} = f(\omega_r, V \le V_L, I \le I_L) \\ i_{sq,L} = f(\omega_r, V \le V_L, I \le I_L) \\ \left(i_{sd,L}\right)^2 + \left(i_{sq,L}\right)^2 \le I_L^2 \end{cases} \qquad (3.3)$$

where the respect of the constraints is verified on the whole angular speed domain of the machine.

Current PI controllers are used in *d,q* frame. Up to the *base* speed value, the magnitude of the air-gap rotor-flux is imposed constant; for greater speeds the drive operates in a very wide field weakening region. Classical space vector modulation is used. At starting, in order to flux the motor avoiding uncontrolled transient, a feed-forward control strategy is applied with hysteresis flux controllers.

3.4 Sensorless strategy for PMSM unit

Figure 3.8 shows the control scheme of PM propulsion unit. Also in this case a field-oriented current-control technique is used. The reference currents i_{sd}^*, i_{sq}^* are evaluated by imposing the maximization of T_e/I_s *torque/current ratio* until the speed base is reached; for greater speed values, a flux weakening strategy is applied. The evaluation of the limit values of i_{sd}, i_{sq} currents is made off-line and the results are placed in a look-up table as shown in (3.3). Standard PI controllers are used.

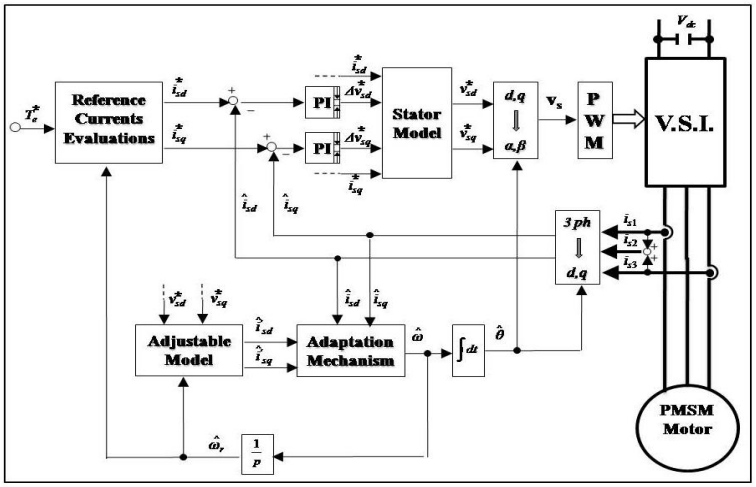

Figure 3.8 **Block diagram of speed sensorless control in PMSM traction drive.**

Model Reference Adaptive scheme is used as speed estimation algorithm ([69],[72]). The reference model, which express the desired performance given a control signal is represented by the PMSM itself, while as adjustable model is chosen the current model of PMSM.

In particular, according to the equations (3.4) in rotary reference frame with d axis coinciding with magnetic axis of PM brushless rotor, i.e.:

$$\begin{cases} v_{sd} = R_s\, i_{sd} + \dfrac{d\phi_{sd}}{dt} - p\omega_r \phi_{sq} \\ v_{sq} = R_s\, i_{sq} + \dfrac{d\phi_{sq}}{dt} + p\omega_r \phi_{sd} \\ \phi_{sd} = L_d\, i_{sd} + \phi_r \\ \phi_{sq} = L_q i_{sq} \end{cases} \qquad (3.4)$$

Selecting as state variables the currents with ($L_d = L_q = L_s$), equations (3.4) can be expressed as follow:

$$\begin{cases} \dfrac{d\, i_{sd}^{'}}{dt} = -\dfrac{R_s}{L_s} i_{sd}^{'} + \omega\, i_{sq}^{'} + \dfrac{v_{sd}^{'}}{L_s} \\ \dfrac{d\, i_{sq}^{'}}{dt} = -\dfrac{R_s}{L_s} i_{sq}^{'} - \omega\, i_{sd}^{'} + \dfrac{v_{sq}^{'}}{L_s} \end{cases} \qquad (3.5)$$

Thus considering angular speed as the adjustable parameter, from equations (3.5) the equations of the adjustable model can be expressed as follow:

$$\begin{cases} \dfrac{d\, \hat{i}_{sd}^{'}}{dt} = -\dfrac{R_s}{L_s} \hat{i}_{sd}^{'} + \hat{\omega}\, i_{sq}^{'} + \dfrac{v_{sd}^{'}}{L_s} \\ \dfrac{d\, \hat{i}_{sq}^{'}}{dt} = -\dfrac{R_s}{L_s} \hat{i}_{sq}^{'} - \hat{\omega}\, i_{sd}^{'} + \dfrac{v_{sq}^{'}}{L_s} \end{cases} \qquad (3.6)$$

Defining the matrices:

$$\mathbf{A}=\begin{pmatrix} -\frac{R_s}{L_s} & \omega \\ -\omega & -\frac{R_s}{L_s} \end{pmatrix};\ \hat{\mathbf{A}}=\begin{pmatrix} -\frac{R_s}{L_s} & \hat{\omega} \\ -\hat{\omega} & -\frac{R_s}{L_s} \end{pmatrix};\qquad \mathbf{B}=\begin{pmatrix} \frac{1}{L_s} \\ \frac{1}{L_s} \end{pmatrix};$$

$\mathbf{u}=\begin{pmatrix} v'_{sd} \\ v'_{sq} \end{pmatrix}$; $\mathbf{D}=\begin{pmatrix} 0 & 1 \\ 1 & 0 \end{pmatrix}$ and then the error and correlation matrix : $\boldsymbol{e}=\boldsymbol{i}'-\hat{\boldsymbol{i}}'$ and $\hat{\mathbf{A}}=\mathbf{A}+\Delta\mathbf{A}$, the equations (3.5) and (3.6) can be written, with $\mathrm{p}=d/dt$ respectively as:

$$\mathrm{p}\,\mathbf{i}'=\mathbf{A}(\hat{\mathbf{i}}'+\mathbf{e})+\mathbf{B}\mathbf{u} \qquad (3.7)$$

$$\mathrm{p}\,\hat{\mathbf{i}}'=\hat{\mathbf{A}}\,\hat{\mathbf{i}}'+\mathbf{B}\mathbf{u} \qquad (3.8)$$

The state space equation (3.7) is subtracted by equation (3.8), leading:

$$\mathrm{p}\,\mathbf{e}=\mathbf{A}\mathbf{e}-\Delta\mathbf{A}\,\hat{\mathbf{i}}' \qquad (3.9)$$

The above equations can be synthesized by the system depicted in Figure 3.9 :

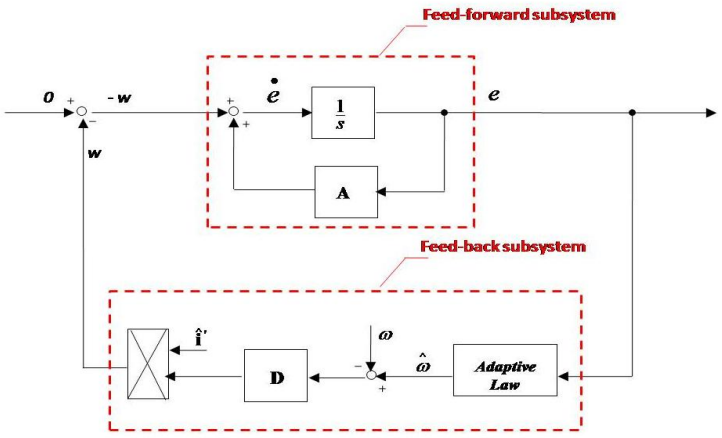

Figure 3.9 **Equivalent feedback structure of PMSM adaptive speed estimator**

The aim is to obtain state error to zero by means of adaptive law when the system is stable. According to Popov hyper stability theorem, two conditions have to be satisfied for the system in Figure 3.9:

1) Transfer function matrix of the linear forward block is positive real strictly.

2) The nonlinear feedback block meets Popov integral inequality, that is:

$$\eta(0,t_1)=\int_0^{t_1} e^T w\,dt \geq -\gamma_0^2 \qquad (3.10)$$

with γ_0 limited positive constant, independent of t_1. Thus, the adaptation mechanism is designed as PI style and described analytically as follow:

$$\begin{cases} \hat{\omega} = k_{p,\omega}\,\varepsilon_\omega + k_{i,\omega}\int_0^t \varepsilon_\omega \,\mathrm{d}t \\ \varepsilon_\omega = \hat{i}_{sd}\,\hat{i}_{sd}' - \hat{i}_{sq}\,\hat{i}_{sq}' - \dfrac{\phi_r}{L_s}(\hat{i}_{sq} - \hat{i}_{sq}') \end{cases} \qquad (3.11)$$

3.5 Numerical Analysis

On the basis of the above mentioned control techniques, simulation investigations are carried out with reference to a case-study of a railway vehicle (see Table 3.1) with two configurations for propulsion units having the main data of Table 3.2. For the sake of simplicity we assume that: the forces acting on the driven axels are equal; there is not slip among them;

equivalent inertia is not affected by the deformation of axels. Therefore, the control loop works with only one motor in the simulative analisys.

In order to evaluate the above described traction units in term of sensorless control and energetic performance, some numerical investigations are performed with a focus on the specific performance of railway traction drives, such as: 1) *operations on the entire speed-domain; 2*) *repowering control* (which occur in the deceleration phase after the inertial slowing down); *3*) *starting from uphill conditions*; 4) *parameter variations of the machine.*

In particular the coasting phase may be obtained by using two different methods of inertial slowing-down:

- reference torque produced by the control strategy is set to zero, while the switching devices of VSI are controlled (*warm coasting*);

- reference torque produced by the control strategy is set to zero, while the switching devices of VSI are open (*cold coasting*).

In the following investigations, acceleration and cruising phases are the same for all the considered cases, while coasting and braking phases are carried out within different time intervals, by considering in all the cases a full electric braking . In particular, starting from an initial speed of the train (that is assumed equal to *60 km/h* in the following sample cases), the transitions from coasting to braking can be fixed at different speed values corresponding to constant flux or field weakening

region and in Table 3.5 are summarized the cases exploited in the next developments.

TABLE 3.5 **Case studies analyzed**

Case	***Coasting***	***Speed interval*** **[** *km/h*]
A1	Warm	60 → **30**
A2	Warm	60 → **45**
B1	Cold	60 → **30**
B2	Cold	60 → **45**

3.5.1 Operations along the overall speed profile

A typical route profile of a light railway vehicle is considered, where in case A1 the coasting duration is long at the expense of braking, that starts at a low train speed of 30 *km*/*h* .

In Fig.3.10 we can easily deduce that, also in presence of fast variations of the reference torque with a *jerk* of 1 m/s^3, the speed-sensorless control of PMSM unit carries out good dynamic performance and the used configuration ensures stable operations either in constant flux or in field weakening region.

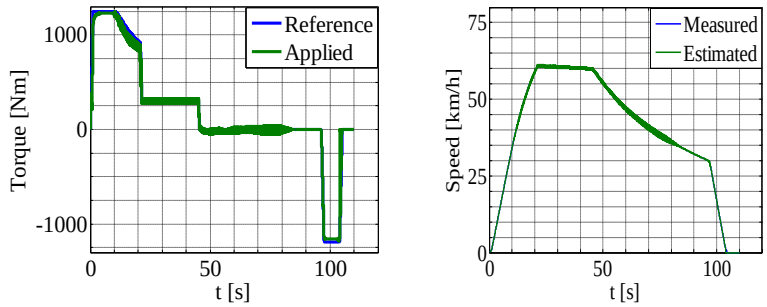

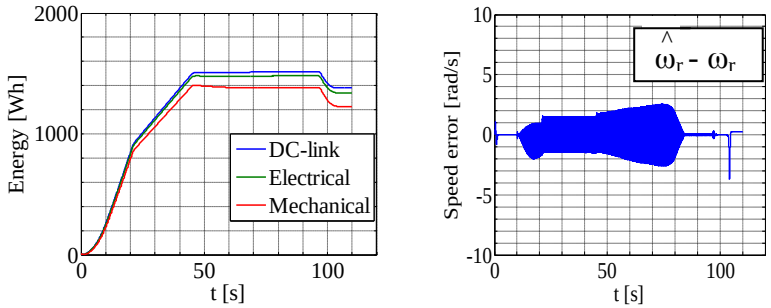

Figure 3.10 **Electromagnetic torque, train speed, energy consumption and rotor speed error versus time, for a traction unit with PM brushless (case A1)**

In Fig.3.11 the time behavior of the same relevant quantities showed in Figure 3.10 are plotted with reference to the IM drive.

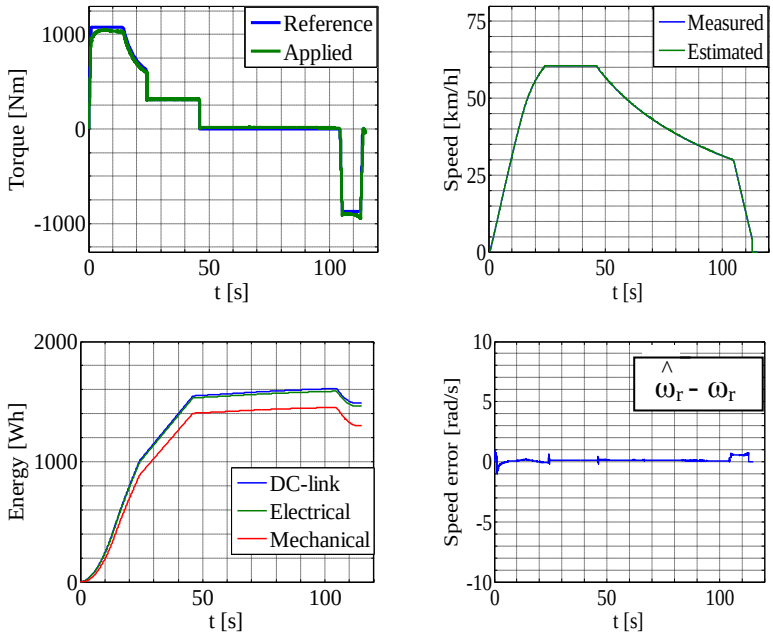

Figure 3.11 **Electromagnetic torque, train speed, energy consumption and rotor speed error versus time, for a traction unit with IM drive (case A1)**

Also in this case the speed - sensorless vector control ensure good dynamic performance on the whole speed domain and with reference to Figure 3.10 better behavior is showed in terms of

speed error estimation and torque oscillations despite in case of in PM brushless drive the switching frequency is higher.

In the case A2, the coasting interval is reduced in favor of braking. The behaviors of torque, speed, energy consumption and rotor speed error are displayed in Fig.s 3.12 and Fig.3.13 for the two configuration considered.

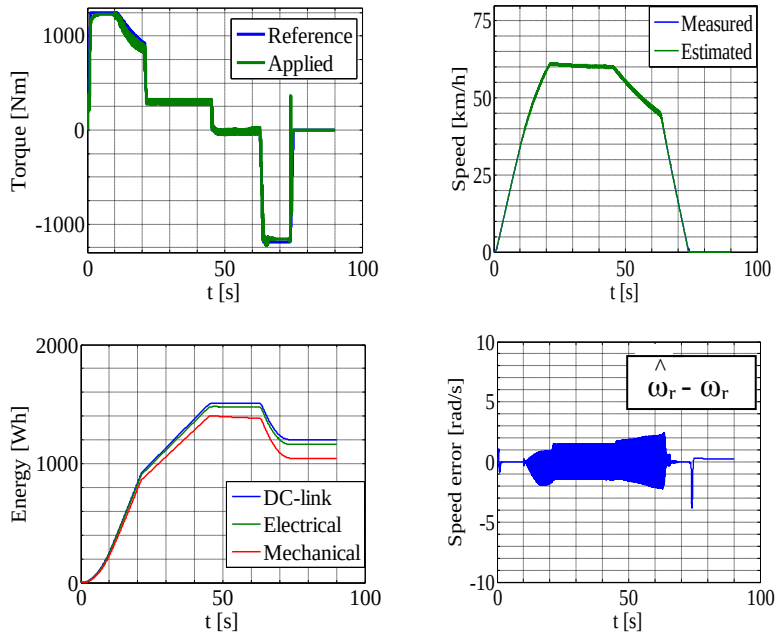

Figure 3.12 **Electromagnetic torque, train speed, energy consumption and rotor speed error versus time, for a traction unit with PM brushless (case A2)**

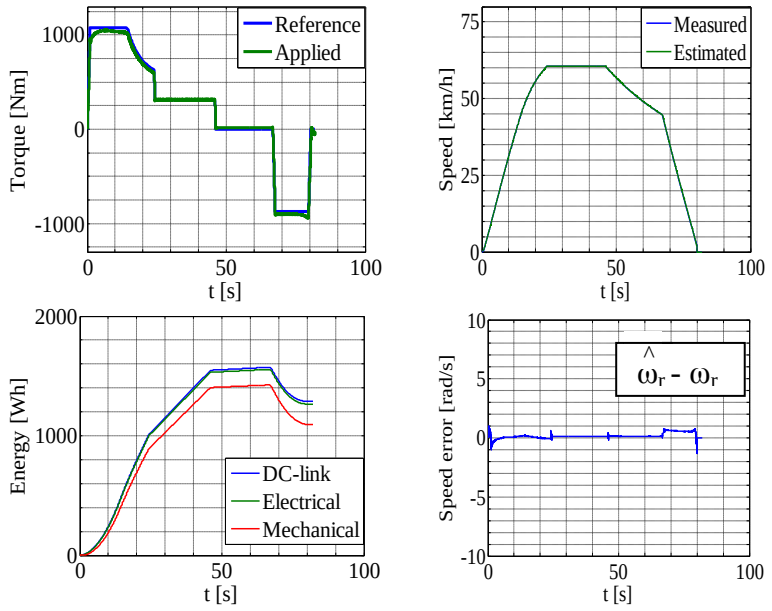

Figure 3.13 **Electromagnetic torque, train speed, energy consumption and rotor speed error versus time, for a traction unit with IM drive (case A2)**

In Fig.s 3.12 and 3.13, the behavior of the two estimators is the same for the two drives as showed in Fig.s 3.10 and 3.11, even if the transition from coasting to braking take place in this case in field weakening operations and showing in general a satisfactory behavior in starting phase at zero-speed, which is one of the most critical conditions.

In case of warm coasting, the inverter is ever operating, also during the deceleration with a reference torque $T_e^* = 0$ and in Table 3.6 are detailed values of energy consumption in different sections of the drives, in case of warm coasting from 60 *km/h* to *30 km/h* (or *45 km/h*) followed by a braking phase until the vehicle stops with constant deceleration of *1 m/s*^{2} for the IM traction unit and *1.1 m/s*^{2} for the PM brushless one.

TABLE 3.6 **Numerical Comparison - Warm Coasting**

Case	Energy consumptiom	Coasting		Braking	
		IM	PMSM	IM	PMSM
A1	dc-link energy [*Wh*]	65.1	16.2	-121.9	-134.7
60→30	Electrical energy [*Wh*]	59.8	6.6	-125.6	-139.8
km/h	Mechanical energy [*Wh*]	52.1	-12.3	-153.2	-155.6
A2	dc-link energy [*Wh*]	29.1	8.4	-283.1	-304.7
60→45	Electrical energy [*Wh*]	27.4	1.9	-288.6	-312.3
km/h	Mechanical energy [*Wh*]	24.9	-13.2	-330.4	-337.6

Since in case of warm coasting the inverter is active, the energy who flows from dc-link to the motor shaft has to balance inverter and motor losses but the deviation from estimated speed to the measured ones involves in torque deviation from the zero reference value, increasing the losses as shown for IM unit.

Instead for PM brushless drive, coasting phase is regenerative; this allows the reduction of energy losses compared to the IM drive. Looking at braking phase, energy efficiencies of PM unit are higher than IM unit, ensuring greater possibilities for energy saving.

Otherwise, in cold coasting the switching devices of the traction inverter are disabled during the coasting interval and currents can be present only in the diodes in case B1 as well as B2. Fig.s 3.14 & 3.15 show the same relevant quantities of Fig.s 3.10 & 3.11 with reference to case B1 and to a traction unit with PM brushless or with IM drive respectively.

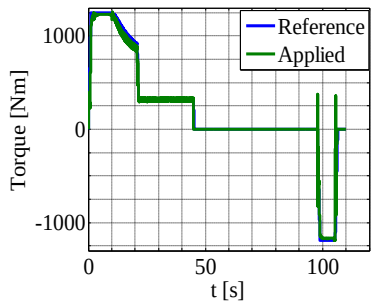

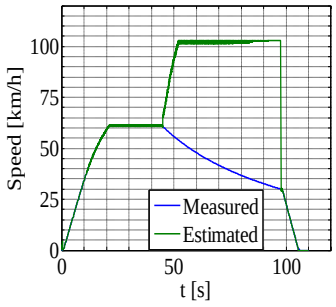

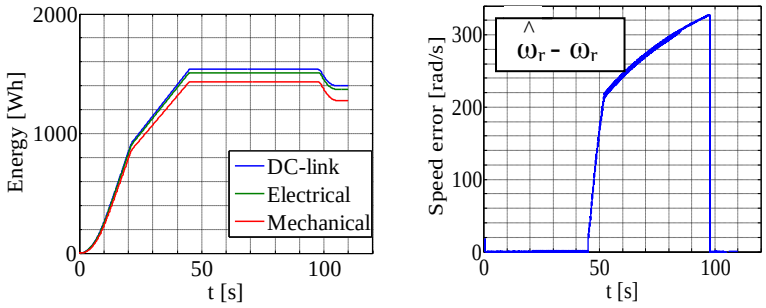

Figure 3.14 **Electromagnetic torque, train speed, energy consumption and rotor speed error versus time, for a traction unit with PM brushless (case B1)**

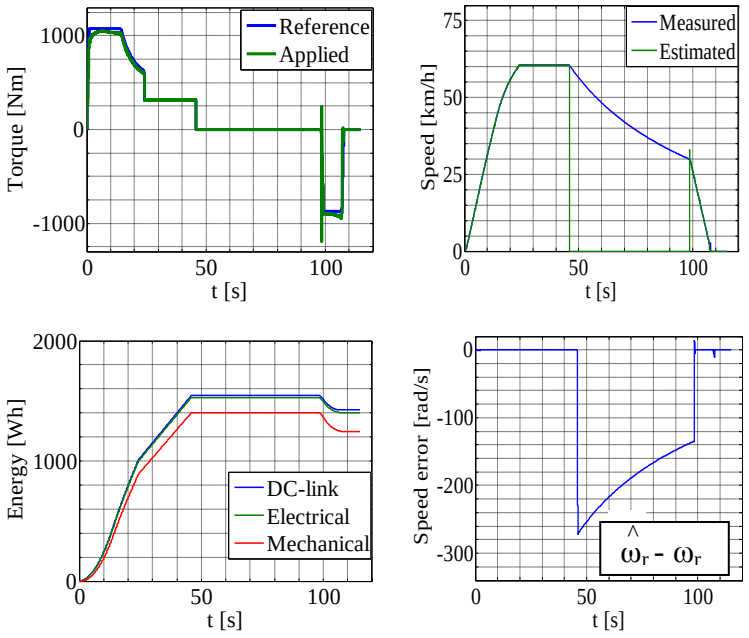

Figure 3.15 **Electromagnetic torque, train speed, energy consumption and rotor speed error versus time, for a traction unit with IM drive (case B1)**

In case of cold coasting with PM or IM unit, the behavior in acceleration and cruising is the same as the case A1, but during the inertial slowing down the estimators involves in deterioration of their performance because the switches are open and the input

currents measured decrease instantaneously to zero. Moreover, transitions from coasting-to-braking are associated to oscillations on the torque.

As already made for the case A2, in Fig.s 3.16 & 3.17 are reported the same quantities debated until now when the transition from inertial slowing down to full electric braking comes out to the speed value of *45 km/h* .

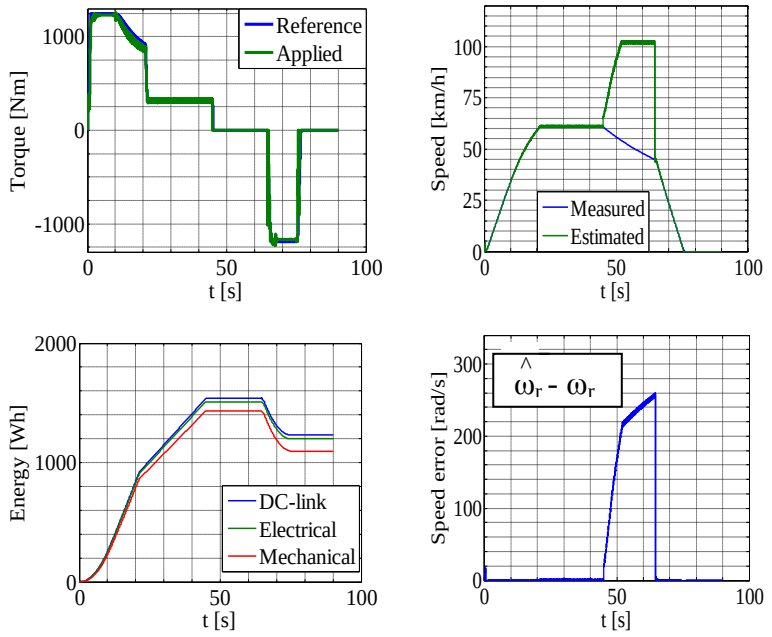

Figure 3.16 **Electromagnetic torque, train speed, energy consumption and rotor speed error versus time, for a traction unit with PM brushless (case B2)**

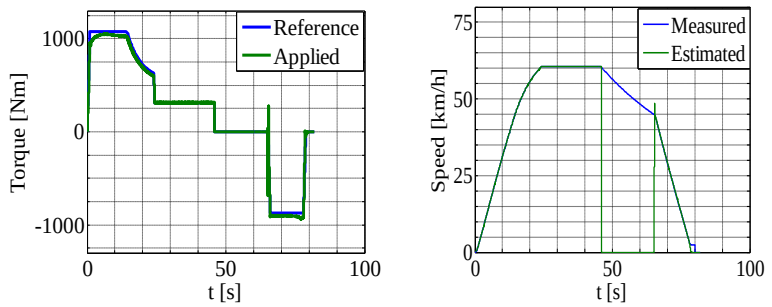

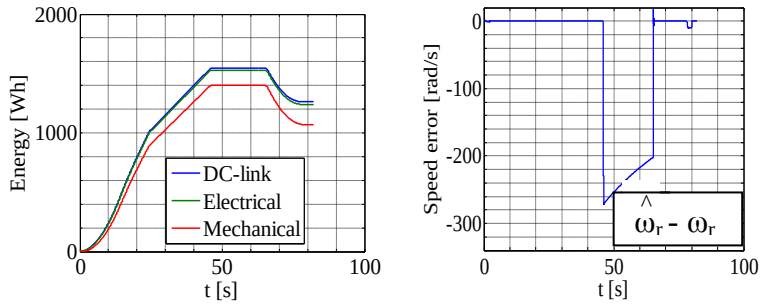

Figure 3.17 **Electromagnetic torque, train speed, energy consumption and rotor speed error versus time, for a traction unit with IM drive (case B2)**

Table 3.7 synthesizes the different energy contributions for the cases B1 and B2.

TABLE 3.7 **Numerical Comparison - Cold coasting**

Case	Energy consumptiom	Coasting		Braking	
		IM	PMSM	IM	PMSM
B1 60→30 *km/h*	dc-link energy [*Wh*]	0.2	0.29	-118	-134.3
	Electrical energy [*Wh*]	~ 0	~ 0	-122.2	-139.6
	Mechanical energy [*Wh*]	~ 0	~ 0	-152.8	-155.6
B2 60→45 *km/h*	dc-link energy [*Wh*]	0.12	0.19	-279.7	-304
	Electrical energy [*Wh*]	~ 0	~ 0	-285.9	-311.8
	Mechanical energy [*Wh*]	~ 0	~ 0	-330.1	-337.5

3.5.2 Repowering Control

For a railway vehicle, the re-powering is a specific situation that may occur after:

- *coasting* operation, when the inverter switching devices are open in order to reduce the commutation/conduction losses;
- a sudden disconnection from the feeding line (pantograph detachment, active operation of protections, …), with the aim to re-establish the drive power.

In the Fig.s 3.18 ÷ 3.22 are displayed the more relevant quantities involved in the repowering analysis, carrying out a zoom on the transitions from coasting to braking for the cases above discussed B1 and B2.

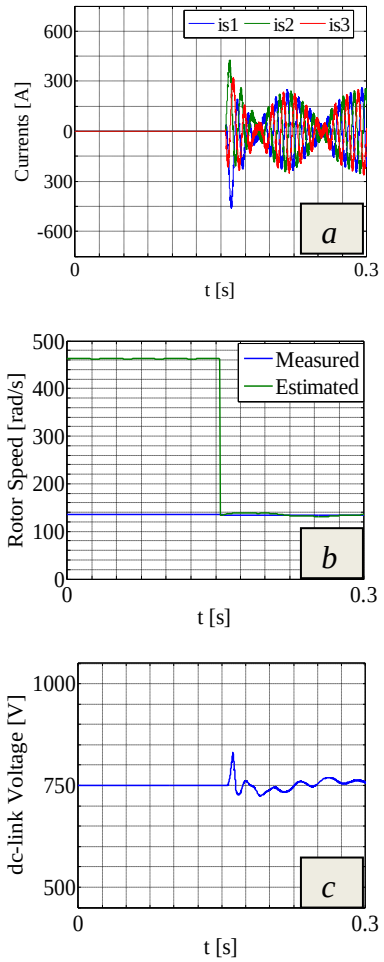

Figure 3.18 **PM brushless unit in repowering (case B1): a) currents ; b) rotor speed ; c) dc-link voltage .**

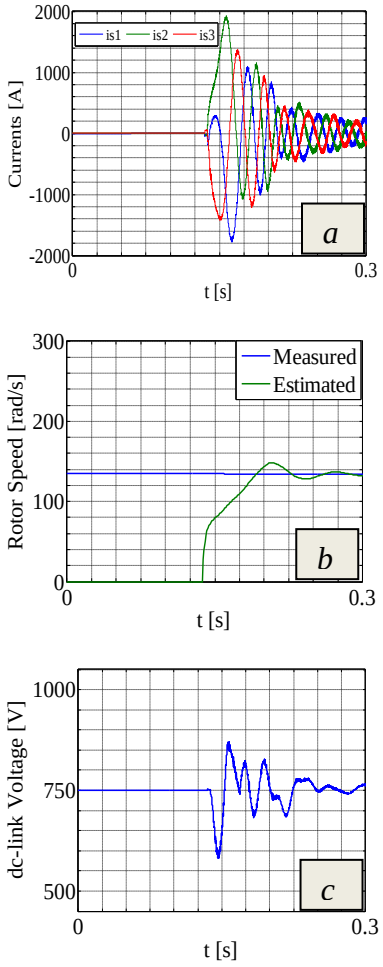

Figure 3.19 **IM unit in repowering (case B1): a) currents ; b) rotor speed ; c) dc-link voltage.**

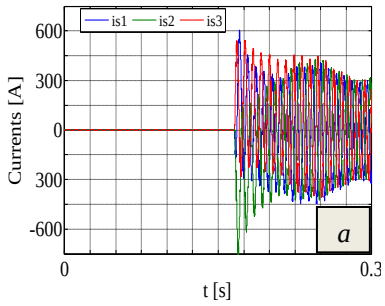

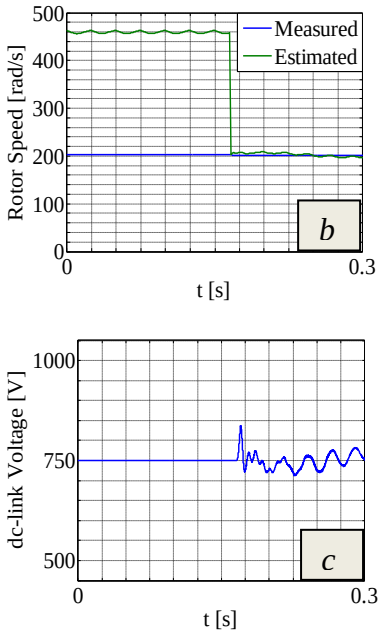

Figure 3.20 **PM brushless unit in repowering (case B2): a) currents ; b) rotor speed ; c) dc-link voltage .**

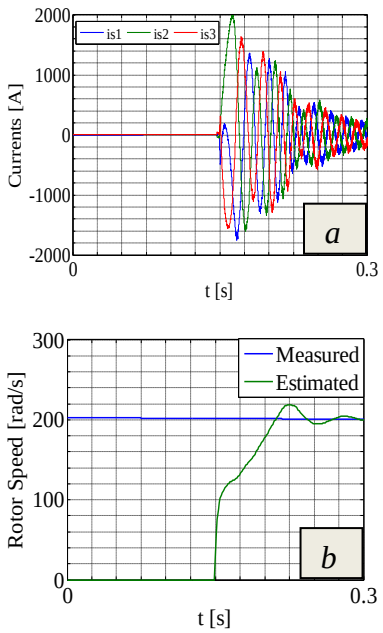

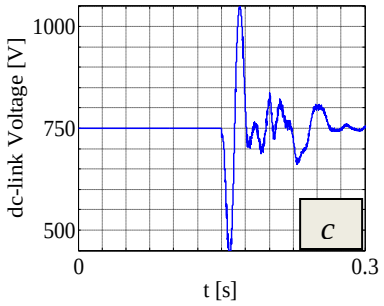

Figure 3.21 **IM unit in repowering (case B2): a) currents ; b) rotor speed ; c) dc-link voltage.**

In the repowering for PM unit, the speed estimator is suitable to ensure stable response for the motor torque and estimated rotor speed both in case B1 and B2 involving in smooth transient in armature currents and dc-link voltage.

Otherwise, the oscillations of the estimated speed for IM unit involve in heavy transient in the armature currents and dc-link voltage which are higher in case B2 than B1; this behavior seems to disagree with the typical threshold values of over-current and over-voltage for the traction drives.

3.5.3 Conditions of Uphill start

One of the most typical operating conditions of a train is the starting from a condition of backward motion, which can occur when the train starts in presence of uphill; consequently, the vehicle crosses the zero-speed region and remains at low speed for a significant time (critical situation for speed-sensorless control).

In Fig.s 3.22 & 3.23 show speed and torque behaviors with reference to a railroad slope of about 30‰ and an initial value of the motor speed of about -10 *rad/s*.

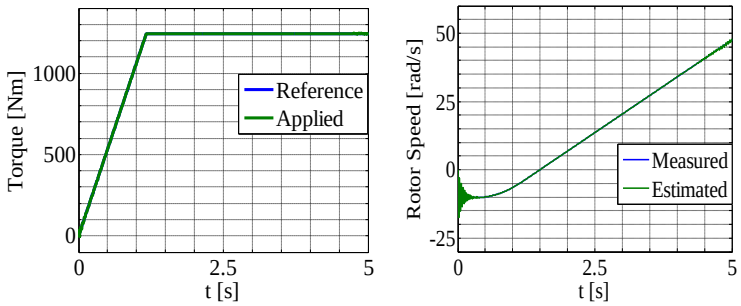

Figure 3.22 **Time behaviour of PM motor Torque and rotor speed, starting from train backward motion.**

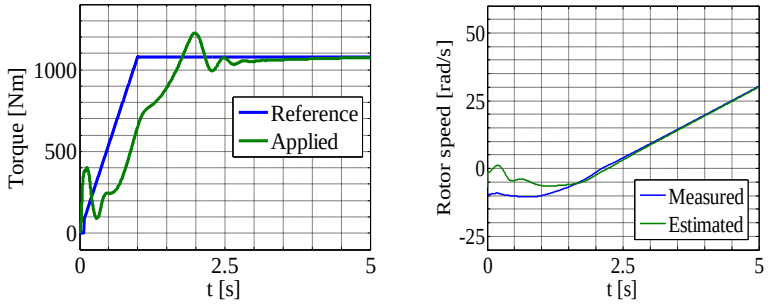

Figure 3.23 **Time behaviour of IM Torque and rotor speed, starting from train backward motion**

The results show better dynamic behavior for PM vehicle; however, in either cases, the crossing of the zero-speed zone is substantially without disturbances and smooth and stable acceleration of the vehicle is guaranteed also when the train starts uphill while it is rolling back.

3.5.4 Machine Parameter Variations

In railway traction systems is required high reliability for a long period and the choice may fall on asynchronous or permanent magnet motors. However, one of the most relevant issue is the change of some parameters during their operations, especially if the machine is operated in overload conditions or for

a long time as is the case of the railway field. The variation of parameters is influenced by the temperature, the iron saturation level, the frequency, etc.; and this is another of the critical aspects to deal with for a speed sensorless control.

In Fig.s 3.24÷3.31 are displayed for the two considered propulsion unit, the diagrams of torque and speed estimation error, taking into account variations of the machine parameters with reference to the rated ones (see Table 3.3) of about ±10% and of ±20% during the operations in low-speed region.

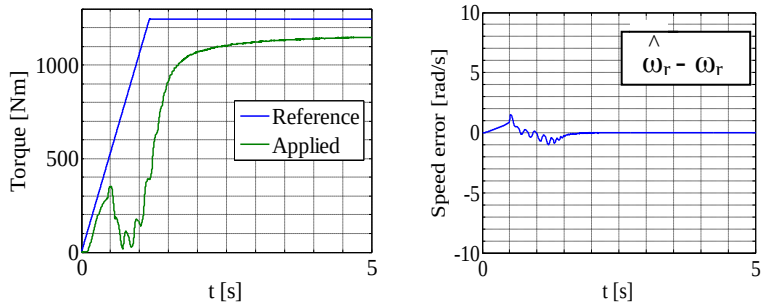

Figure 3.24 **Time behaviour of Torque and rotor speed error of PM unit with the increase of 10% for L_s and R_s**

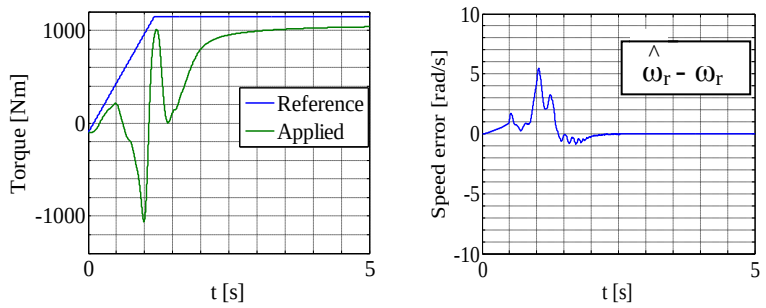

Figure 3.25 **Time behaviour of Torque and rotor speed error of PM unit with the increase of 20% for L_s and R_s**

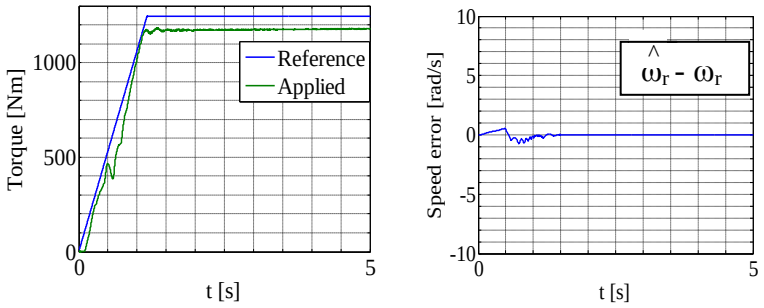

Figure 3.26 **Time behaviour of Torque and rotor speed error of PM unit with the decrease of 10% for L_s and R_s**

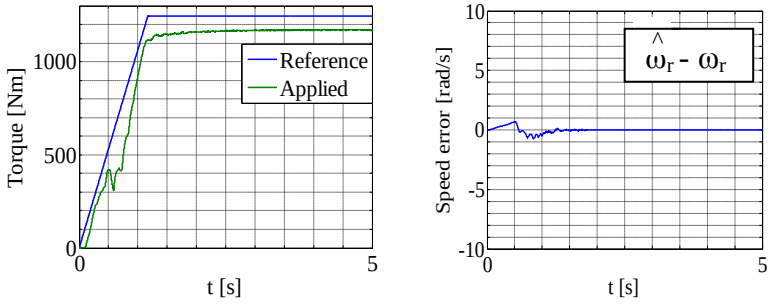

Figure 3.27 **Time behaviour of Torque and rotor speed error of PM unit with the decrease of 20% for L_s and R_s**

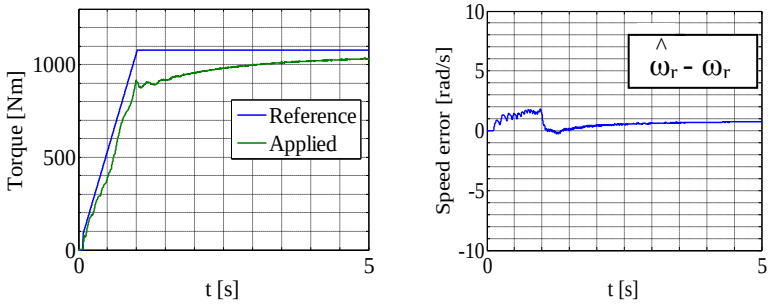

Figure 3.28 **Time behaviour of Torque and rotor speed error of IM unit with the increase of 10% for R_s , $R_r^{'}$ and L_m**

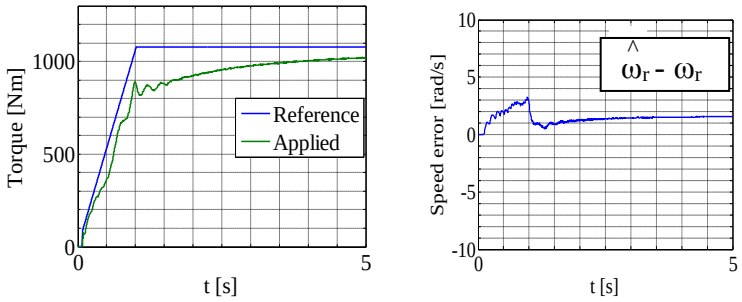

Figure 3.29 **Time behaviour of Torque and rotor speed error of IM unit with the increase of 20% for R_s, R_r' and L_m**

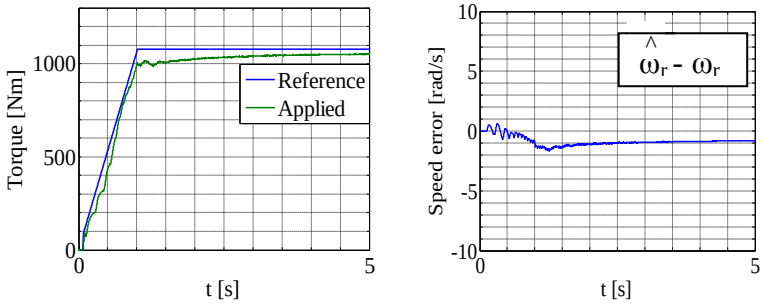

Figure 3.30 **Time behaviour of Torque and rotor speed error of IM unit with the decrease of 10% for R_s, R_r' and L_m**

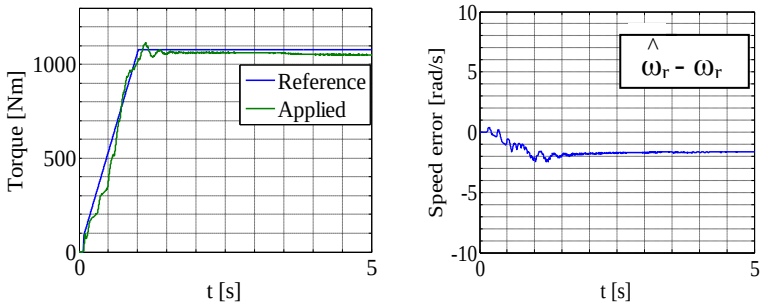

Figure 3.31 **Time behaviour of Torque and rotor speed error of IM unit with the decrease of 20% for R_s, R_r' and L_m**

It is worth of mentioning that the errors on the estimated speed are limited at appropriate values for railway traction applications

which makes their operation suitable. The change of the parameters, influence speed estimation error especially at starting phase when the fast variations of the reference torque with a jerk of $1\ m/s^3$ occurs. The increment affect the speed sensorless control more than their decrease. In particular, Fig. 3.25 and 3.29 show the deterioration of torque dynamic performance in case of +20% ; on the contrary, a restricted steady-state error on the torque is ensured in all the conditions.

Conclusions

In this thesis work, different strategies have been explored and a design methodology has been proposed to improve energy efficiency and reliability of light railway transportation systems. In particular, two main topics have been analyzed: one refers to the possibility to use Supercapacitors Energy Storage System (SESS) in light railway systems; the second one refers to specific applications of sensorless control of traction units. About SESS, after a preliminary analysis of the storage technologies available on the market, they have been considered in *on board* configuration for a vehicle prototype, introducing a method to optimize their design in order to achieve different routes in catenary free-operations. After that, a *stationary* configuration of SESS has been considered, with reference to a demonstrator of a metro rail system set in the test room of Hitachi Rail Italy, where a control strategy has been carried out for energy flow management in non receptive DC grid. The second topic refers to the introduction of two sensorless control strategies for two different railway traction architectures using IM and/or PMSM drives, paying attention to energetic and dynamic performance in different specific operating conditions required by the railway traction drives.

The experimental results show the fulfillment of the mission and then the feasibility of the proposed methodology in terms of values of capacitance, weight and sizes of SESS for the considered vehicle, which performs different routes with different lengths and slopes in catenary free operations.

Moreover, experimental results show the effectiveness of the proposed control strategy for stationary configuration of SESS,

evaluating the benefits achievable in terms of energy saving, power peak shaving, voltage profile optimization, reduction of losses on the feeding line and reduction of braking chopper operations.

On the other hand, an extensive numerical analysis has been carried out for the two different traction architectures proposed using two kinds of speed sensorless vector control; the results have shown better performance of PM brushless vehicle in terms of efficiency and capability to recover energy, especially during coasting and braking intervals.

Nevertheless, sensorless control of PMSM drive produces higher oscillations in speed estimation during the ordinary operations on the entire speed domain. This is mainly due to the intrinsic characteristics of the PM brushless machines considered for this traction applications, which present low values of stator inductance.

In case of backward conditions, good results are obtained in both configurations ensuring the running operations; in repowering operations, PMSM sensorless control shows better dynamic performance, avoiding undesired transients on phase currents and dc-link voltage which on the contrary occur in case of IM sensorless drive.

The sensitivity parameter analysis highlights that good immunity to the machine parameter variations is ensured for the sensorless strategies proposed where the decrease of the performance is more evident when the values of parameters increase.

Further developments could be represented by :

- experimental tests with the two traction architectures presented, in order to verify and validate performance and different behaviors for the sensorless strategies proposed;
- experimental on-line tests for a light railway system which includes some SESS devices, investigating the effectiveness of the control strategy proposed in a real system.

Acknowledgments

I want to express my gratitude to my tutor Prof. Andrea Del Pizzo and my co-tutor Ph.D. Eng. Luigi Fratelli for giving me this opportunity.

Moreover I am full of gratitude for the company Hitachi Rail Italy S.p.A.; in particular I am grateful to Roberta Schiavo, Danilo De Vita, Guglielmo Navarra, Fabio Voccia and Pasquale Capasso for their precious support in these years.

I also thank Ciro Nappo and Roberto Frasca for their cooperation with experimental tests sections carried out on a real vehicle prototype.

I want to say thank you to Luigi Pio Di Noia, for his assistance with the writing and his availability.

I want to say thank you to my love, Nunzia, for encouraging me continuously and for her patience.

At the end, none of this would be possible without my family; I am immensely grateful for their unconditioned love and support, in good and bad times.

References

[1] Cascetta E., "Transportation Systems Engineering: Theory and Methods",Vol.49. *University of Naples,*Federico II, 2001.

[2] ERRAC, The European Rail Research Advisory Council Rail route 2050: TheSustainable Backbone of the Single European Transport Area. Available on-line:http://www.errac.org/wp-content/uploads/2013/11/D9-SRRA-RAILROUTE2050.pdf .

[3] APTA, Resource Library: Fact Book Glossary, (Online). Available: http://www.apta.com/resources/statistics/Pages/glossary.aspx, (accessed 2013).

[4] Kondo, K.; "Recent Energy Saving Technologies on Railway Traction Systems". *IEEJ Trans. On Electric and Electronics Engineering*, vol. 5, pp. 298÷303.

[5] Bucherl, D.; Nuscheler, R.; Meyer, W.; Herzog, H., "Comparison of electrical machine types in hybrid drive trains: Induction machine vs. permanent magnet synchronous machine" *18th Intern. Conf. on Electrical Machines, ICEM 2008*, pp. 1÷6, Sept. 2008.

[6] Melfi, M. J.; Evon, S.; McElveen, R., "Permanent magnet motors for power density and energy savings in industrial applications", *Conf. Record of 54th Annual Pulp and Paper Industry Technical Conf., PPIC 2008*, pp. 218÷225, June 2008.

[7] Del Pizzo, A.; Iannuzzi, D.; Spina, I, "High performance control technique for unbalanced operations of single-VSI dual-PM brushles motor drives", *IEEE Intern. Symposium on Industrial Electronics, ISIE 2010*; Bari (Italy); pp. 1302÷1307, July 2010.

[8] Eun-Kyu Lee, "Traction technologies for railways in Korea" International Power Electronics Conference (IPEC), Sapporo (Japan), pp. 2849÷2852, 21÷24 June 2010.

[9] Yano, M.; Iwahori, M., "Transition from slip-frequency control to vector control for induction motor drives of traction applications in Japan", *5th Intern. Conf. on Power Electronics and Drive Systems, PEDS 2003*, vol. 2, pp. 1246÷1251, Nov. 2003.

[10] Oettmeier, M.; Spichartz, M.; Staudt, V.; Steimel, A., "Stator-flux-oriented control of PMSM in traction - Experimental results", *Electrical Systems for Aircraft, Railway and Ship Propulsion (ESARS)*, Bologna (Italy), pp. 1÷6, 16÷18 Oct. 2012.

[11] Peroutka, Z.; Zeman, K.; Krus, F.; Kosta, F., "Control of permanent magnet synchronous machine wheel drive for low-floor tram", *13th European Conf. on Power Electronics and Applications, EPE '09*, Barcelona (Spain), pp. 1÷9, Sept. 2009.

[12] Weckert, M.; Roth-Stielow, J., "Chances and limits of a thermal control for a three-phase voltage source inverter in traction applications using permanent magnet synchronous or induction machines", *14th European Conf. on Power Electronics and Applications (EPE 2011)*, Birmingham (U.K.), pp. 1÷10, Aug. 2011.

[13] Acampa M. S. D.; Del Pizzo, A.; Rizzo, R.,"A control algorithm of AC-Brushless drives for railways traction application", *IEEE-ACEMP2007, Aegean Conf. on Electric Machines, Power Electro-nics and Electromotion*, Bodrum (Turkey), pp.33÷38, Sept. 2007.

[14] Demmelmayr, F.; Troyer, M.; Schroedl, M., "Advantages of PM-machines compared to induction machines in terms of efficiency and sensorless control in traction applications", *IECON 2011 - 37th Annual Conf. on IEEE Industrial Electronics Society*, Melbourne (Australia), pp. 2762÷2768, 7÷10 Nov. 2011.

[15] Wei Wang; Bouscayrol, A.; Ming Cheng, "Comparison of two different traction systems for subway application using Energetic Macroscopic Representation" *Conf.* on *Vehicle Power and Propulsion (VPPC) IEEE* , pp. 984÷989, 9÷12 Oct. 2012.

[16] Beneduce, L.; Cascone, B.; Del Pizzo, A.; Fratelli, L.; Spina, I., "Comparative analysis of performance and energy losses in light

railways vehicles equipped with IM or PMSM drive", *Proc. of SPEEDAM 2014*, Ischia (Italy), pp. 566÷572, 18÷20 June 2014.

[17] Brando, G.; Dannier, A.; Del Pizzo A.; Perna, D., "Energetical comparative analysis of IM and PM-brushless drives in light railway transportation systems", 2016 International Symposium on Power Electronics, Electrical Drives, Automation and Motion (SPEEDAM), Anacapri (Italy), pp. 1160-1165, 22÷24 June 2016.

[18] Franke, R.; Terwiesch, P.; Meyer, M., "An algorithm for the optimal control of the driving of trains", Proceedings of the 39th IEEE Conference on Decision and Control, vol.3, pp. 2123-2128, 2000.

[19] Moon-Ho Kang, "A GA-based Algorithm for Creating an Energy-Optimum Train Speed Trajectory", Journal of International Council on Electrical Engineering, Vol. 1, No. 2, pp. 123-128, 2011.

[20] Colak, K.; Czarkowski, D.; de Leon, F., "Energy minimization forcatenary-free mass transit systems using Particle Swarm Optimization", Electrical Systems for Aircraft, Railway and Ship Propulsion (ESARS), pp. 1-5, 2012.

[21] Chang, C.; Sim, S., "Optimising train movements through coast control using genetic algorithms", IEE Proceedings on Electric Power Applications, vol. 144, pp. 65‑73, 1997.

[22] Gunselmann, W., "Technologies for increased energy efficiency in railway systems", *European Conference on Power Electronics and Application*s, pp. 10÷15, 2005.

[23] López-López, Á. J.; Pecharromán, R.R.; Fernández-Cardador, A.; Paloma Cucala, A., "Assessment of energy-saving techniques in direct-current-electrified mass transit systems", Transportation Research Part C: Emerging Technologies, Volume 38, Pages 85-100, January 2014.

[24] Hillmansen, S.; "Electric railway traction systems and techniques for energy saving", *Electric Traction Systems, IET Professional Development Course on*, 2012, pp. 19-23.

[25] Barrero, R.; van Mierlo, J.; Tackoen, X., "Energy savings in public transport", IEEE on Vehicular Tchnology Magazine, Vol. 3, pp. 26- 36, 2008.

[26] Del Pizzo, A.; Fratelli, L.; Nappo, C.; Perna, D., "A method for 'design to range' energy storage systems in catenary free operations of light railway vehicles", *5th Intern. Conference on Clean Electrical Power ICCEP 2015*, pp. 761÷766, 4 Aug. 2015.

[27] Kondo, K.; Yuki, K.; Terauchi, N.; Hasebe, T., "Evaluation of induction motor speed sensorless control for railway vehicle traction system", *European Conference on Power Electronics and Applications*, pp.4÷8, 11÷14 Sept. 2005.

[28] Kang, J.; Zeng, X.; Wu Y.; Hu, D., "Study of position sensorless control of PMSM based on MRAS," IEEE International Conference on Industrial Technology, Gippsland,VIC, pp.1-4, 2009.

[29] Burke, A., "Ultracapacitor technologies and application in hybrid and electric vehicles", International Journal of Energy Resources, n.34, pp. 133÷151, 2010.

[30] Barrero, R.; Tackoen, X.; Van Mierlo J., "Improving Energy Efficiency in Public Transport: Stationary supercapacitor based energy storage systems for a metro-network", Proc. of Vehicle Power and Propulsion Conf. VPPC'08, Harbin, China, pp. 1÷8, Sept. 2008. http://www.euromatic.no/ZEBRA_Aug17.pdf

[31] Vazquez, S.; Lukic, S.M.; Galvan, E.; Franquelo, L. G.; Carrasco, J. M.: "Energy Storage Systems for Transport and Grid Applications", Industrial Electronics, IEEE Transactions on , vol.57, n.12, pp. 3881÷3895, Dec. 2010.

[32] Ibrahim, H.; Ilinca, A.; Perron, J., “Energy storage systems - Characteristics and comparisons”, Renewable and Sustainable Energy Reviews, vol. 12, n. 5, pp. 1221÷1250, May 2007.

[33] Barrero, R.; Tackoen, X.; Van Mierlo, J., "Stationary or onboard energy storage systems for energy consumption reduction in a metro network", *Proc. Inst. Mech. Eng. Pt. F: J Rail Rapid Transit*, vol. 224 (3), pp. 207–225, Jan. 2010.

[34] Barrero, R.; Tackoen, X.; Van Mierlo J., “Improving Energy Efficiency in Public Transport: Stationary supercapacitor based energy storage systems for a metro-network”, Proc. of Vehicle Power and Propulsion Conf. VPPC’08, Harbin, China, pp. 1÷8, Sept. 2008.

[35] Sepe, R. B.; Steyerl, A.; Bastien, S. P., "Lithium-ion supercapacitors for pulsed power applications", Energy Conversion Congress and Exposition (ECCE), pp.1813÷1818, 17÷22 Sept. 2011.

[36] Du Pasquier, A.; Plitz, I; Menocal, S.; Amatucci, G., “A comparative study of Li-ion battery, supercapacitor and nonaqueous asymmetric hybrid devices for automotive applications”, Journal of Power Sources, Volume 115, Issue 1, pp. 171÷178, 27 March 2003.

[37] Khaligh, A.; Li, Z., "Battery, Ultracapacitor, Fuel Cell, and Hybrid Energy Storage Systems for Electric, Hybrid Electric, Fuel Cell, and Plug-In Hybrid Electric Vehicles: State of the Art," in IEEE Transactions on Vehicular Technology, vol. 59, no. 6, pp. 2806-2814, July 2010.

[38] Ratniyomchai, T.; Hillmansen, S.; Tricoli, P., "Recent developments and applications of energy storage devices in electrified railways," Electrical Systems in Transportation, IET , vol.4, n.1, pp.9÷20, March 2014.

[39] Okui, A., Hase, S., Shigeeda, H., Konishi, T. and Yoshi, T. "Application of energy storage system for railway transportation in

Japan," The 2010 International Power Electronics Conference - ECCE ASIA -, pp. 3117-3123, Sapporo, 2010.

[40] Konishi, T., Morimoto, H., Aihara, T. and Tsutakawa, M.," Fixed Energy Storage Technology Applied for DC Electrified Railway", IEEJ Trans Elec Electron Eng, 5: 270–277, 2010.

[41] http://www.euromatic.no/ZEBRA_Aug17.pdf .

[42] Radcliffe, P., Wallace, J. S. and Shu, L. H. "Stationary applications of energy storage technologies for transit systems," 2010 IEEE Electrical Power & Energy Conference, Halifax, NS, pp. 1-7, 2010.

[43] Glickenstein, H. "Contactless payment debuts on London's buses, new and improved railways around the world [Transportation Systems]," in IEEE Vehicular Technology Magazine, vol. 8, no. 2, pp. 19-25, June 2013.

[44] Conway, B. E., "Electrochemical Supercapacitors – Scientific Fundamentals and Technological Applications". New York, Kluwer Academic / Plenum Publishers, 1999.

[45] Miller, J. M., "Ultracapacitor Applications". The Institution of Engineering and Technology, UK, 2011.

[46] Musolino,V., "Supercapacitor storage systems: modeling, control strategies,applications and sizing criteria". Ph.D. Thesis in Electrical Engineering, XXVI Cycle,Electrical Department, Polytechnic of Milan, Italy, supervisor Tironi E., 2011.

[47] Ciccarelli, F., "Energy management and control strategies for the use of supercapacitors storage technologies in urban rayilway traction systems". Ph.D. Thesis in Electrical Engineering, XXVI Cycle,Department of Electrical Enginnering and Information Technology, University of Naples "Federico II", Italy, supervisor Iannuzzi D., 2014.

[48] Namisnyk, A. M., " A survey of electrochemical supercapacitor technology". Ph.D Thesis in Electrical Engineering, University of Technology, Sydney, Supervisor: Jian Guo Zhu., 2003.

[49] Čihak, E.E.T.; Jakopović, E.E.Z, " Supercapacitors in power converter DC link: A short overview of design and application issues. *Proc. 34th Int. convention on informationand communication technology, electronics and microelectronics MIPRO 2011*, Opatija; Croatia; pp. 130-135, 23-27 May 2011.

[50] Musolino, V.; Piegari L.; Tironi, E., "New Full-Frequency-Range Supercapacitor Model With Easy Identification Procedure," IEEE Transactions on Industrial Electronics, vol. 60, no. 1, pp. 112-120, Jan. 2013.

[51] Barcellona, S.; Ciccarelli, F.; Iannuzzi D.; Piegari, L., "Modeling and Parameter Identification of Lithium-Ion Capacitor Modules," in IEEE Transactions on Sustainable Energy, vol. 5, no. 3, pp. 785-794, July 2014

[52] Devillers, N.; Jemei, S.; Péra, M.; Bienaimé, D.; Gustin, F., "Review of characterization methods for supercapacitor modelling ", *J Power Sources*, vol. 246, pp. 596-608, 2014.

[53] Spyker, R.L.; Nelms, R.M., "Classical equivalent circuit parameters for a double-layercapacitor", *IEEE Transactions on Aerospace and Electronic Systems*, vol. 36 (3 –PART1), pp.829-836, 2000.

[54] Maxwell Technologies. 125 V heavy transportation module. Available on-line: http://www.maxwell.com/products/ultracapacitors/docs/125vmodule_ds_1014696-7.pdf (Accessed 2013).

[55] Steiner, M.; Klohr, M.; Pagiela, S., "Energy storage system with ultracaps on board of railway vehicles," Power Electronics and Applications, 2007 European Conference on , pp.1÷10, 2÷5 Sept. 2007.

[56] Wang, W.; Cheng, M.; Wang, Y.; Zhang, B.; Zhu, Y., Shichuan Ding ; Chen, W., "A Novel Energy Management Strategy of Onboard Supercapacitor for Subway Applications With Permanent-Magnet Traction System," in IEEE Transactions on Vehicular Technology, vol. 63, no. 6, pp. 2578-2588, July 2014.

[57] Iannuzzi, D.; Tricoli, P., "Speed-Based State-of-Charge Tracking Control for Metro Trains With Onboard Supercapacitors," Power Electronics, IEEE Transactions on , vol.27, no.4, pp.2129,2140, April 2012

[58] Iannuzzi, D.; Lauria, D.; Tricoli, P., "Optimal Design of Stationary Supercapacitors Storage Devices for Light Electrical Transportation Systems", *Journal of Optimization and Engineering*, vol. 13 (4), pp. 689-704, Dec. 2012.

[59] Ciccarelli, F.; Iannuzzi, D.; Lauria, D., "Stationary ultracapacitors storage device for improving energy saving and voltage profile of light transportation networks", *Transportation Research Part C: Emerging Technologies*, vol. 21 (1), Jan. 2012, pp. 321-337.

[60] Clemente, G.; Fantauzzi, M.; Lauria, D., "Energy savings in urban mass transit systems: A probabilistic approach for sizing electric energy storage devices", *Proc. 4th Int. Conf. on Clean Electrical Power ICCEP 2011*, Alghero, Italy, 11-13, pp. 610-613, June 2013.

[61] Foiadelli, F.; Roscia, M.; Zaninelli, D., "Optimization of storage devices for regenerative braking energy in subway systems", Proc. *IEEE Power Engineering Society General Meeting PES 2006*, Montreal, QC, Canada, 18-22 June 2006.

[62] Barrero, R., Tackoen, X., Van Mierlo, J., "Quasi-static simulation method for evaluation of energy consumption in hybrid light rail vehicles", Proc. *Vehicle Power Propulsion Conf. VPPC 2008*, Harbin, China, September 3-5, 2008.

[63] Ciccarelli, F., Iannuzzi, D., Kondo, K. and Fratelli, L. "Line-Voltage Control Based on Wayside Energy Storage Systems for Tramway Networks," in *IEEE Transactions on Power Electronics*, vol. 31, no. 1, pp. 884-899, Jan. 2016.

[64] Levine, W. , "The Control Handbook", Piscataway, NJ: IEEE Press,1996.

[65] Erickson, R. W.; Maksimovic, D., "Fundamentals of Power Electronics", Norwell, MA: Kluwer, 2002.

[66] Ciccarelli, F.; Iannuzzi. D.; Spina, I., "Comparison of Energy Management Control Strategy based on Wayside ESS for LRV application", *Proc. 39th Annual Conference of the IEEE Industrial Electronics Society IECON2013*, Vienna, Austria, 10-14 Nov., pp. 1548-1554, 2013.

[67] Allegre, A.-L.; Bouscayrol, A.; Delarue, P.; Barrade, P.; Chattot, E.; El-Fassi, S., "Energy Storage System With Supercapacitor for an Innovative Subway," Industrial Electronics, IEEE Transactions on , vol.57, no.12, pp.4001,4012, Dec. 2010

[68] Lhomme, W.; Delarue, P.; Barrad, P.; Bouscaroy, A.; Rufer, A., "Design and control of a supercapacitor storage system for traction applications," in Conf. Rec. IEEE IAS Annu. Meeting, pp. 2013–2020, 2005.

[69] Vas P., "Sensorless vector and direct torque control",Vol. 729. Oxford University Press, Oxford, UK, 1998.

[70] Ogawa T.; Ishida, S.; Kojima, T.; Sato, T.; Taguchi, H.; Ohashi, S., "Speed sensorless vector control for rolling stock", European Conference on Power Electronics and Applications, pp. P1÷P7, 11-14 Sept. 2005.

[71] Bocker, J.; Mathapati, S., "State of the art of induction motor control", IEEE- IEMDC'07, vol.2, pp.1459÷1464, 3÷5 May 2007.

[72] Bingyi, Z.; Xiangjun, C.; Guanggui, S.; Guihong, F., "A Position Sensorless Vector-control System Based on MRAS for Low Speed and High Torque PMSM Drive," 2005 International Conference on Electrical Machines and Systems, Nanjing, pp.1682-1686, 2005.

[73] Schauder, C., "Adaptive speed identification for vector control of induction motors without rotational transducers", *IEEE Trans. IA 28-5*, Sept/Oct, pp. 1054÷1061, 1992.

[74] Holtz, J., "Sensorless control of induction machines - with or without signal injection?", *IEEE Trans.on IE*, 53-1, pp. 7÷30, Feb 2006.

[75] Zhang, Y.; Zhao, Z.; Lu, T.; Yuan, L.; Xu, W.; Zhu, J., ”A comparative study of Luenberger observer, sliding mode observer and extended Kalman filter for sensorless vector control of induction motor drives”, *Energy Conversion Congress and Exposition, IEEE*, pp. 2466÷2473, 2009.

[76] Ohyama, K.; Asher, G. M.; Sumner M., ”Comparative analysis of experimental performance and stability of sensorless induction motor drives”, *IEEE Transactions on Industrial Electronics*, 53(1): pp. 178÷186, 2006.

[77] K. Kondo, "PMSM and IM rotational sensorless technologies specialized for railway vehicles traction," 2014 IEEE 5th International Symposium on Sensorless Control for Electrical Drives, Hiroshima, 2014, pp. 1-7.

[78] Bolognani, S.; Oboe, R.; Zigliotto, M., "Sensorless full-digital PMSM drive with EKF estimation of speed and rotor position," in IEEE Transactions on Industrial Electronics, vol. 46, no. 1, pp. 184-191, Feb 1999

[79] Joohn-Sheok Kim and Seung-Ki Sul, "High performance PMSM drives without rotational position sensors using reduced order observer," Industry Applications Conference, 1995. Thirtieth IAS Annual Meeting, IAS '95., Conference Record of the 1995 IEEE, Orlando, FL, pp. 75-82 vol.1 1995.

[80] Walambe, R. A.; Joshi, V. A.; Apte, A. A.; Kolhe J. P.; Deshpande, A., "Study of sensorless control algorithms for a permanent magnet synchronous motor vector control drive," 2015 International Conference on Industrial Instrumentation and Control (ICIC), Pune, pp. 423-428,2015.

[81] Haddoun, A.; Benbouzid, M. E. H.; Diallo, D.; Abdessemed, R.; Ghouili, J.; Srairi, K., "Comparative analysis of estimation

techniques of SFOC induction motor for electric vehicles", *18th International Conference on Electrical Machines*, 2008. ICEM 2008, pp. 1÷6, Vilamoura, 2008.

[82] Kondo, K.; Yuki, K.; Terauchi, N.; Hasebe, T., "Evaluation of induction motor speed sensorless control for railway vehicle traction system", *European Conference on Power Electronics and Applications, 2005*, pp.4÷8, 11÷14 Sept. 2005.

[83] Ogawa, T.; Ishida, S.; Kojima, T.; Sato, T.; Taguchi, H.; Ohashi, S., "Speed sensorless vector control for rolling stock", *European Conference on Power Electronics and Applications*, pp. 7÷14, 11÷14 Sept. 2005.

[84] Tsuji, M.; Chen, S.; Kai, T.; Del Pizzo, A.; Yamada, E.; Hamasaki, S., "A precise torque and high efficiency control for Q-axis flux-based induction motor sensorless vector control system", *Proc. of SPEEDAM'06*, Taormina (Italy), pp. 990-995, May 2006.